จลนศาสตร์การตกผลึกเย็นที่สภาวะอุณหภูมิคงที่และสัณฐานวิทยาของฟิล์มพอลิแลคติกเอซิดโดยการเติมสารตัวเติม

นางสาวสุพัตรา โชคศรีวิจิตร

วิทยานิพนธ์นี้เป็นส่วนหนึ่งของการศึกษาตามหลักสูตรปริญญาวิศวกรรมศาสตรมหาบัณฑิต
สาขาวิชาวิศวกรรมเคมี ภาควิชาวิศวกรรมเคมี
คณะวิศวกรรมศาสตร์ จุฬาลงกรณ์มหาวิทยาลัย
ปีการศึกษา 2558

Isothermal cold-crystallization kinetics and morphology of PLA sheet with the incorporation of fillers

Miss Suphattra Choksriwichit

A Thesis Submitted in Partial Fulfillment of the Requirements
for the Degree of Master of Engineering Program in Chemical Engineering
Department of Chemical Engineering
Faculty of Engineering
Chulalongkorn University
Academic Year 2015

Thesis Title	Isothermal cold-crystallization kinetics and morphology of PLA sheet with the incorporation of fillers
By	Miss Suphattra Choksriwichit
Field of Study	Chemical Engineering
Thesis Advisor	Associate Professor Anongnat Somwangthanaroj, Ph.D.
Thesis Co-Advisor	Assistant Professor Wanchai Lerdwijitjarud, Ph.D.

Accepted by the Faculty of Engineering, Chulalongkorn University in Partial Fulfillment of the Requirements for the Master's Degree

.....Dean of the Faculty of Engineering
(Associate Professor Supot Teachavorasinskun, D.Eng.)

THESIS COMMITTEE

.....Chairman
(Professor Paisan Kittisupakorn, Ph.D.)

.....Thesis Advisor
(Associate Professor Anongnat Somwangthanaroj, Ph.D.)

.....Thesis Co-Advisor
(Assistant Professor Wanchai Lerdwijitjarud, Ph.D.)

.....Examiner
(Associate Professor Siriporn Damrongsakkul, Ph.D.)

.....External Examiner
(Sunan Tiptipakorn, D.Eng.)

สุพัตรา โชคศรีวิจิตร : จลนศาสตร์การตกผลึกเย็นที่สภาวะอุณหภูมิคงที่และสัณฐานวิทยาของฟิล์มพอลิแลคติกเอซิดโดยการเติมสารตัวเติม (Isothermal cold-crystallization kinetics and morphology of PLA sheet with the incorporation of fillers) อ.ที่ปรึกษาวิทยานิพนธ์หลัก: รศ. ดร. อนงค์นาฏ สมหวังธนโรจน์, อ.ที่ปรึกษาวิทยานิพนธ์ร่วม: ผศ. ดร. วันชัย เลิศวิจิตรจรัส, 91 หน้า.

งานวิจัยนี้มีวัตถุประสงค์เพื่อศึกษาจลนศาสตร์การตกผลึกเย็นที่สภาวะอุณหภูมิคงที่และสัณฐานวิทยาของฟิล์มพอลิแลคติกเอซิดโดยการเติมสารตัวเติมและการปรับปรุงพื้นผิวของสารตัวเติมโดยใช้สารควบคู่ไซเลน งานนี้ทำการศึกษาผลของชนิดของสารตัวเติม ปริมาณของสารตัวเติม และอุณหภูมิการอบหลังการขึ้นรูปที่มีต่อสัณฐานวิทยา สมบัติทางความร้อน และสมบัติเชิงกล โดยชิ้นงานฟิล์มขึ้นรูปด้วยวิธีเทอร์โมฟอร์มมิ่ง ผลการวิเคราะห์เชิงความร้อนด้วยเทคนิค DSC พบว่าสารตัวเติมส่งผลให้อุณหภูมิการเกิดผลึกเย็น (T_{cc}) ของฟิล์มคอมโพสิทลดลงต่ำกว่าของฟิล์มพอลิแลคติกเอซิด เนื่องจากสารตัวเติมเป็นสารก่อผลึกที่ช่วยเร่งอัตราการเกิดผลึกของฟิล์มพอลิแลคติกเอซิด การเติมทัลก์ที่ปริมาณ 5 เปอร์เซ็นต์โดยปริมาตร ทำให้อัตราการเกิดผลึกเร็วที่สุดที่อุณหภูมิในการเกิดผลึก 100 องศาเซลเซียส ในการปรับปรุงสมบัติเชิงกลของฟิล์มคอมโพสิท พบว่าทัลก์และแคลเซียมคาร์บอเนตส่งผลให้มีค่าความต้านทานแรงดึงและค่ามอดูลัสภายใต้แรงดึงสูงกว่าของฟิล์มพอลิแลคติกเอซิด และเมื่อเติมทัลก์ที่ผ่านการปรับปรุงพื้นผิว ช่วยเพิ่มการกระจายของสารตัวเติม เพิ่มอันตรกิริยาระหว่างทัลก์และเมตริกซ์ของ ฟิล์มพอลิแลคติกเอซิดมากขึ้น นอกจากนี้สมบัติเชิงกลของฟิล์มพอลิแลคติกเอซิด/ทัลก์ที่ผ่านการปรับปรุงพื้นผิวมีสมบัติเปลี่ยนแปลงน้อยมาก

ภาควิชา	วิศวกรรมเคมี	ลายมือชื่อนิสิต	.....
สาขาวิชา	วิศวกรรมเคมี	ลายมือชื่อ อ.ที่ปรึกษาหลัก	.....
ปีการศึกษา	2558	ลายมือชื่อ อ.ที่ปรึกษาร่วม	.....

5770337021 : MAJOR CHEMICAL ENGINEERING

KEYWORDS: POLYLACTIC ACID / THERMOFORMING / COLD CRYSTALLIZATION

SUPHATTRA CHOKSRIWICHIT: Isothermal cold-crystallization kinetics and morphology of PLA sheet with the incorporation of fillers. ADVISOR: ASSOC. PROF. ANONGNAT SOMWANGTHANAROJ, Ph.D., CO-ADVISOR: ASST. PROF. WANCHAI LERDWIJITJARUD, Ph.D., 91 pp.

The research aimed to enhance the isothermal cold-crystallization kinetics and morphology of poly(lactic acid) (PLA) sheet by an incorporation of filler as nucleating agent and the chemical surface modification of filler by silane coupling agent. The effects of filler type, content and isothermal annealing temperature on morphology, thermal and mechanical properties of PLA sheet were investigated. Sheets of PLA composites were thermoformed using a thermoforming machine. The thermal analysis from differential scanning calorimetry (DSC) showed that cold crystallization temperature (T_{cc}) of the PLA composites was lower than that of neat PLA, suggesting that filler acted as nucleating agent accelerating the crystallization rate of PLA. Adding talc at 5 vol% provided the fastest isothermal crystallization rate of PLA at 100°C. It was also found that incorporation of talc and $CaCO_3$ increased tensile strength and Young's modulus of the PLA composites. Moreover, the PLA composites containing silane-treated talc at 5 vol% showed the improvement of filler dispersion, which increased the interfacial area and interaction between talc and PLA matrix. In addition, the mechanical properties of treated filler/PLA composite film did not significantly change much upon film stretching.

Department:	Chemical Engineering	Student's Signature .....
Field of Study:	Chemical Engineering	Advisor's Signature .....
Academic Year:	2015	Co-Advisor's Signature .....

ACKNOWLEDGEMENTS

I would like to express my sincere thanks to my thesis advisor, Associate Professor Dr. Anongnat Somwangthanaroj and my co-advisor, Assistant Professor Dr. Wanchai Lerdwijitjarud for precious advice, guidance and support throughout my research thesis and editing of this thesis.

I am great appreciate to the chairman, Professor Dr. Paisan Kittisupakorn, and committee members, Associate Professor Dr. Siriporn Damrongsakkul and Dr. Sunan Tiptipakorn who provided significant suggestions and valuable recommendations for this research.

In addition, I am grateful to everyone in the Polymer Engineering Research Laboratory, Department of Chemical Engineering, Chulalongkorn University, for discussion and friendly encouragement and given comments. Furthermore, I would like to thank my friends, Dr. Chavakorn Samthong for his kind help with editing my thesis and answered my questions all the times.

The financial support of this work is under the Institutional Research Grant (The Thailand Research Fund), IRG 5780014, and Chulalongkorn University, Contract No. RES_57_411_21_076.

Finally, I would like to wholeheartedly give all gratitude to the members of my family for their generous encouragement during my entire studies. Also, every person who deserves thanks for the encouragement and support that cannot be listed.

CONTENTS

Page

Page

Page

LIST OF FIGURES

LIST OF TABLES

LIST OF ABBREAVIATIONS

ΔH_c	Enthalpy of crystallization
ΔH_{cc}	Enthalpy of cold-crystallization
ΔH_m	Enthalpy of melting
ΔH^o_m	Enthalpy of melting of perfect crystalline polymer
DSC	Differential scanning calorimetry
k	Temperature-dependent crystallization rate constant
n	Avrami index
PLA	Poly(lactic acid)
POM	Polarized optical microscopy
SEM	Scanning electron microscopy
$t_{1/2}$	Crystallization half-time
T_c	Crystallization temperature
T_{cc}	Cold-crystallization temperature
T_m	Melting temperature
X_c	Relative degree of crystallinity

CHAPTER I

INTRODUCTION

1.1 General Introduction

Currently, biopolymers have been widely used in various applications such as breathable film packaging and scaffold for medical purpose. Biopolymers include poly(lactic acid) (PLA), poly(butylene adipate-co-terephthalate) (PBAT), poly(butylene succinate) (PBS), polyhydroxyalkanoates (PHAs) and so forth. PLA is a biodegradable aliphatic polyester produced from sugar, corn and rice, which are renewable resources, to replace the petroleum-based plastics. PLA has high transparency, high strength, high modulus, biodegradability, and biocompatibility. However, neat PLA is brittle and has poor melt strength and slow crystallization rate, limiting its usage.

Polylactic acid (PLA) has been used in packaging due to its biodegradability and its similarity of properties of polyethylene terephthalate (PET) such as high transparency. Some packaging is not focused on the mechanical properties depending on applications. Thermoforming process includes the annealing process of polymer. The study on the crystallization rate is in order to decrease the thermoforming cycle time as increasing production rate. The crystallization rate of PLA can be improved by an incorporation of nucleating agent, i.e., montmorillonite clay, natural rubber (NR), calcium carbonate ($CaCO_3$), talc and corn starch [1-5]. The effect of these fillers on the melt-crystallization as well as mechanical and thermal properties of the polymer

composites has been extensively investigated by many researchers [6-8]. Nevertheless, the poor dispersion of filler in the polymer matrix is a critical issue that needs to be solved to optimize the properties of the polymer composites; thus, the chemical surface modification by grafting chemicals onto the filler surface is required to improve the filler dispersion [9-11].

Another approach to increase the degree of crystallinity of polymer is by annealing the polymer at the certain temperature between its glass transition temperature (T_g) and melting temperature (T_m). For the slow-crystallizing PLA, this annealing process can increase the degree of crystallinity from the isothermal cold-crystallization mechanism. The annealing polymer is by thermoforming process. Cold-crystallization is an important crystallization process of PLA upon heating the polymer above its glass transition temperature that considerably affects the total crystallinity and final properties of the polymer. Therefore, the cold-crystallization kinetics of the polymer should be studied to control the crystallization rate as well as crystallization morphology of the PLA composites under the isothermal cold-crystallization condition.

In this study, the crystallization rate and crystallinity of PLA will be improved by adding fillers as nucleating agents and annealing PLA under the isothermal cold-crystallization condition at 90, 100, 110, 120 and 130°C. The effect of incorporation of talc, $CaCO_3$, and cassava starch on the thermal properties and cold-crystallization behavior will be examined by differential scanning calorimetry (DSC) and polarized optical microscopy (POM). Avrami model will also be used to evaluate the cold-

crystallization mechanism under the isothermal condition. Further, the morphology of the PLA composites will be observed by scanning electron microscopy (SEM). The mechanical properties of PLA composites prepared by cast-film extrusion and thermoforming process will be investigated using a universal testing machine. Chemical surface modification of filler will be performed to improve the interaction between filler and PLA matrix. Functional groups on the filler surface will be confirmed by Fourier transform infrared (FTIR) spectroscopy.

1.2 Objectives

1. To investigate the effect of talc, $CaCO_3$, and starch in the PLA composites on the morphology, thermal properties, isothermal cold-crystallization behavior, and mechanical properties.

2. To evaluate the effect of chemical surface modification of filler with 3-aminopropyltriethoyxsilane (APTES) and vinyltriethoyxsilane (VTES) on the morphology, thermal properties, isothermal cold-crystallization behavior, and mechanical properties of the PLA composites.

1.3 Scopes of the research

1. The content of talc, $CaCO_3$ and starch will be varied at 1, 3, 5, 7 and 10 percent by volume (vol%).

2. The isothermal cold-crystallization kinetics will be studied at 90, 100, 110, 120 and 130 $^{\circ}C$.

3. Parameters to achieve the PLA composites with the fastest isothermal cold-crystallization rate including crystallization temperature, type of filler and filler content from the first part will be selected for the second part - functionalization of filler with 3-aminopropyltriethoyxsilane (APTES) and vinyltriethoyxsilane (VTES).

4. The mechanical properties of PLA composites from the cast-film extrusion and thermoforming process will be studied.

CHAPTER II

THEORY AND LITERATURE REVIEWS

2.1 Poly (lactic acid)

Poly(lactic acid) (PLA) is a biodegradable aliphatic thermoplastic polyester derived from the polycondensation or ring-opening polymerization of L-lactic acid and D-lactic acid, which are produced from the carbohydrate fermentation of renewable resources such as sugar cane, rice and corn. The molecular structure of PLA is shown in Figure 2.1.

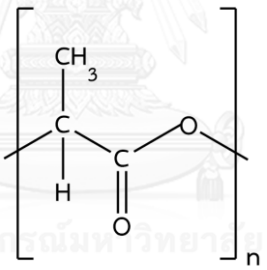

Figure 2. 1 Molecular structure of PLA

Unfortunately, PLA has some drawbacks such as brittleness, poor melt strength and slow crystallization rate, affecting the physical and mechanical properties as well as the processability of PLA. The general properties of PLA used in this work are summarized in Table 2.1.

Table 2.1 Properties of PLA (grade: 2003D; NatureWorks LLC)

Properties	**Value**
Tensile Strength	53 MPa
Tensile modulus	3.5 GPa
Tensile elongation	6.0 %
Heat distortion temperature	55 ^{o}C
Density	1.24 g/cm^{3}
Melt mass-flow rate, 210^{o}C, 2.16 kg)	6 g/10 min
Melting temperature, T_m	144-155 ^{o}C
Glass transition temperature, T_g	55-65 ^{o}C

2.2 Annealing mechanism

The annealing process can change the crystal structure, degree of crystallinity, perfection of crystals and the orientation of both crystalline and amorphous phase of the polymer. Annealing of polymer is influenced by crystallization time as well as crystallization temperature between the glass transition temperature (T_g) and melting temperature (T_m). For example, annealing of poly(ethylene terephthalate) (PET) in a temperature range between 68 to 75^{o}C, which is below T_g of PET, showed no formation of crystal rearrangement due to the quenched polymer chains in a glassy state. Annealing the polymer at cold crystallization temperature (T_{cc}) for a long time period resulted in the structural transformation of crystal from less perfect to more perfect structure. Figure 2.2 displays three temperature regimes of crystallization zone.

In regime I, at low crystallization temperature near T_g, the crystal growth rate is slow because the annealing state is not far from the glassy state at which the polymer chains are frozen. The crystal growth rate gradually increases as the temperature increases owing to high mobility of polymer chains. In regime II, the crystallization of polymer from the melting state to growing crystals depends on the temperature. In regime III, at higher temperature, the amorphous component gets high energy and tends to diffuse into the melt, inhibiting the crystal growth rate considerably [12].

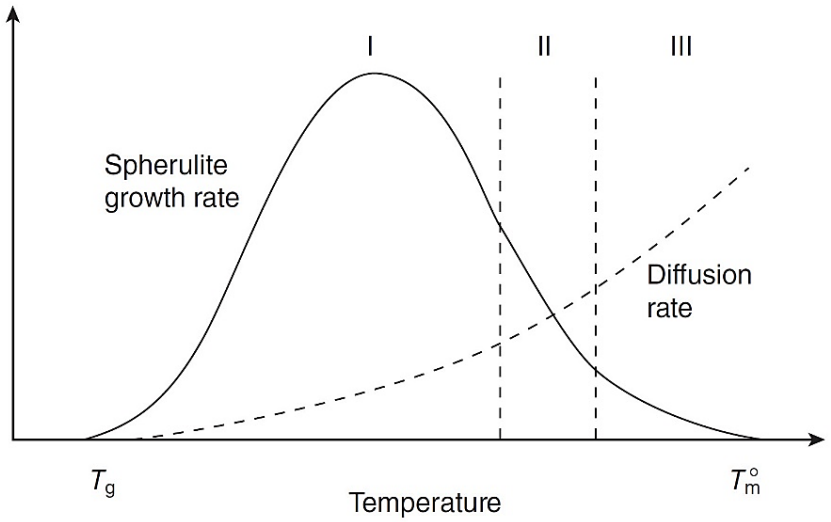

Figure 2.2 Three temperature regimes for crystallization of crystallizable polymer [12]

2.3 Crystallization mechanism

The crystallization process contains two steps, i.e., nucleation and crystal growth. The molten polymer molecule forms a crystal nuclei composed of nanometer-sized ordered polymer chains owing to the variation of heat motion or additional

heterogeneous crystal seeds. The nucleation density depends on the additives, nature of polymer, and temperature. The polymer chains orderly fold and grow as a function of time, leading to larger crystal size until the crystals impinge on one another. The growth of polymer crystal can be one-, two- and three dimension.

Generally, PLA can be crystallize of in several forms; i.e., α, β and γ, depending on the processing condition. The most common and stable polymer can be developed from the melt or solution under normal conditions. The α-form grows upon the conditions such as melt, cold and solution crystallization. Recently, α'-form of PLA with the same conformation to α-form but difference in packing manner is also observed. A crystal α'-form of PLA is formed when crystallization temperature (T_c) is below 110°C but the α-form is formed when T_c is above 120°C, and the mixture of α' and α-forms are formed when $110^{\circ}C \leq T_c \leq 120^{\circ}C$ [7, 13]. In case of PLA, there are two types of crystallization, i.e., melt crystallization and cold crystallization. The detail of crystallization of PLA is discussed as follows.

2.3.1 Melt crystallization

Melt crystallization is the intrinsic property of semi-crystalline polymer, in which the molten polymers crystallize from the melt to reduce the total surface free energy, leading to the formation of the crystal structure from the amorphous structure. The formation of crystal depends on the crystallization temperature (T_c) of the polymers [14]. According to previous works, the exothermic peak of melt crystallization

of injection molded neat PLA was absent, indicating that the cooling rate during the DSC measurement was very fast and thus the molten PLA chains did not have enough time to crystallize, leading to 100% amorphous PLA. It was found that an incorporation of elastomer enhanced the melt crystallization; this reflected by the appearance of exothermic peak and a shift of melt crystallization temperature (T_{mc}) to higher temperature. Furthermore, the enthalpy of melt crystallization (ΔH_{mc}) decreased and T_{mc} shifted to lower temperature as the cooling rate increased, as expected [15]. Moreover, the study on the isothermal crystallization kinetics from the melt of PLA/10 wt% PHB blend showed the decrease of the cold crystallization temperature with the increase of talc content higher than 0.5 phr, accelerating the crystallization rate of neat PLA. Besides, the activation energy (ΔE) for PLA/10 wt% PHB/0.5 phr talc (108 kJ mol^{-1}) was higher than that of PLA/ 10 wt% PHB (70 kJ mol^{-1}) due to the nucleating effect of talc particle. However, the performance of talc as nucleating agent of PLA was always restricted because of the agglomeration of talc particles in the PLA matrix[16]. In addition, the crystal growth of PLA blended with 1.2 wt% talc was measured by a polarized optical microscope (POM) as illustrated in Figure 2.3. The spherulite of PLA/1.2 wt% talc was smaller than that of neat PLA because talc particles increased the number of crystal nuclei [13]. As evaluated by the Avrami index (n) of neat PLA which was in ranges of 2.4-3, the crystal growth mechanism of neat PLA was three-dimension [17, 18].

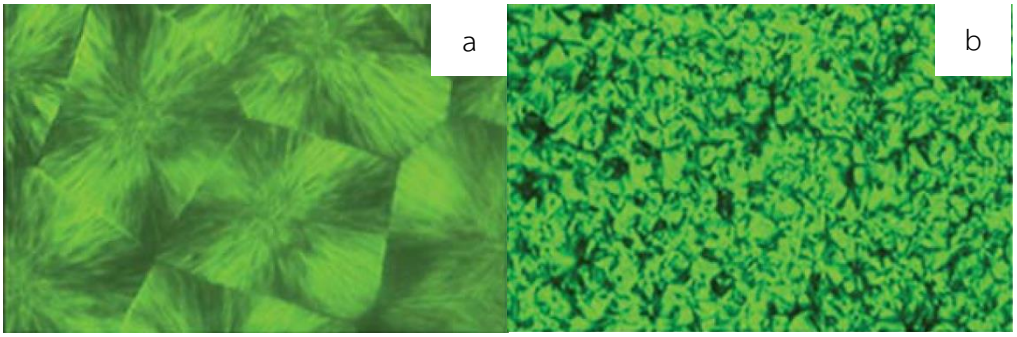

Figure 2.3 POM micrographs of growth crystals of PLA sample of (a) the neat PLA and (b.) PLA/1.2 wt% talc [13]

2.3.2 Cold crystallization

Cold crystallization is the characteristic of polymer above the glass transition temperature. Cold crystallization is an exothermic process of polymer upon heating from the glassy state, which results in an orderly crystalline structure. Annealing upon isothermal cold-crystallization at temperature below T_m of polymer increased the degree of structural order. The cold crystallization has been investigated by many researchers [15, 19-22]. At temperature of 104°C, the cold crystallization rate of PLA was approximately 5 times of melt crystallization rate. The activation energies of cold crystallization and melt crystallization were 173±8.9 kJ mol^{-1} and 109.6±8.8 kJ mol^{-1}, respectively [17].

PET, which was undergone the cold crystallization process, had high degree of crystallinity, leading to high Young's modulus, high tensile strength and low deformation at break [20]. The structure of the glassy amorphous PET depended on

the cooling rate. The kinetics of cold crystallization of PET showed three-dimensional crystal growth. In the isothermal cold-crystallization, the overall crystallization rate from the Avrami model showed the same trend as the experimental data [23]. The cold crystallization of PLA with compressed carbon dioxide showed that CO_2 enhanced the crystallization rate with increasing pressure in a range of 0-4 MPa, resulting in an increased mobility of the polymer chains in solid state [24]. In addition, for the PLA blends with elastomer 30 wt% prepared by injection molding process, the elastomer hindered the crystal growth of PLA owing to high levels of free volume. Further, increasing cooling rate resulted in quenching of PLA chains to form crystal, leading the shift of cold crystallization temperature to higher temperature. In contrast, annealing of PLA under isothermal cold crystallization condition resulted in decreased enthalpy of cold crystallization (ΔH_{cc}) and higher degree of crystallinity. As shown in Figure 2.4, the crystallization half time ($t_{1/2}$), where fractional crystallinity equals to 0.5, of PLA decreased with increasing isothermal cold crystallization temperature, implying the faster cold-crystallization rate [15].

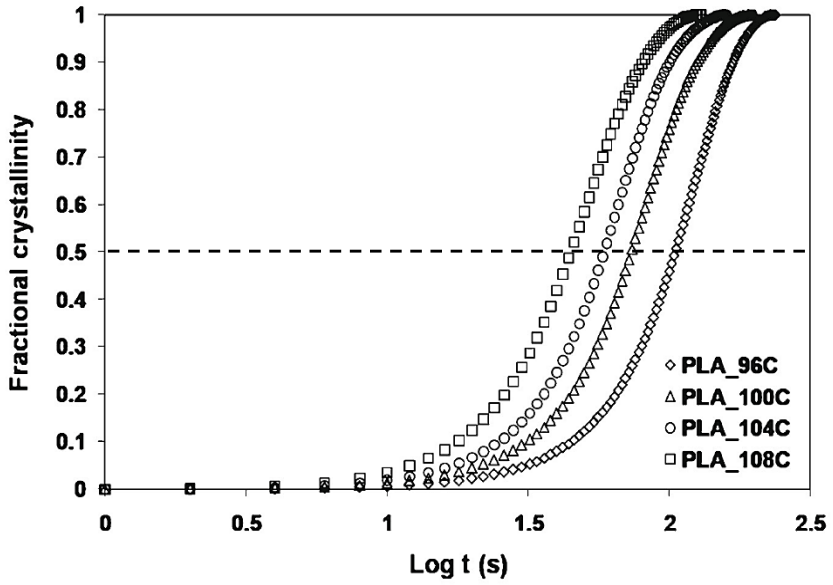

Figure 2.4 Fractional crystallinity vs isothermal crystallization temperature of neat PLA [15]

In addition, the crystallization kinetics parameters were also calculated in order to describe the cold-crystallization mechanism by using Avrami model. The Avrami model is widely used to determine the isothermal and non-isothermal crystallization kinetics of polymer. The Avrami equation is expressed as follows:

$$1\text{-}X_c(t) = \exp(-kt^n) \quad (1)$$

By linearization of equation (1), taking a double logarithm to convert the Avrami equation to equation (2)

$$\log [-\ln(1\text{-}X_c(t))] = \log(k) + n\log(t) \quad (2)$$

where X_c is the time-dependent relative volumetric crystallinity. k is crystallization rate constant that concludes the temperature dependent terms, and nucleation rates. n is Avrami index (Avrami exponent). Another important parameter is half-time of crystallization ($t_{1/2}$), defined as the time required to obtain 50% of total crystallinity from cold-crystallization process which can be obtained according to the following formula:

$$t_{1/2} = (\ln 2/k)^{1/n} \quad (3)$$

The Avrami index (n) is composed of two terms:

$$n = n_d + n_n \quad (4)$$

where n_d represents the dimensionality of the growing crystals and this quantity can only have the values of 1, 2 or 3 corresponding to one-, two- or three-dimensional entities that are formed. The time dependence of the nucleation is represented by n_n. In principle, its value should be either 0 or 1, where 0 corresponds to instantaneous nucleation and 1 corresponds to sporadic nucleation [25].

2.4 Enhancement of crystallization of PLA

2.4.1 Annealing upon cold crystallization

Annealing affects the mobility of the chain in the crystalline phase [14]. The non-equilibrium state can be manifested itself by imperfect crystals and/or constrained amorphous phase. Annealing at elevated temperature promotes the chain

movement of the constrained amorphous phase. The schematic drawing of PLA samples before and after annealing at elevated temperature is illustrated in Figure 2.5 [26]. Increasing annealing temperature of PET increased the crystallization rate. Meanwhile, the maximum value of the enthalpy referred to the highest degree of crystallinity during heating [27]. The exothermic peak corresponded to the crystallization of amorphous regions. The observed T_g increased slightly with annealing time [28]. Furthermore, PLA after annealing at temperature of 80°C had the degree of crystallinity increased from 3.3% (10 minutes) to 21.0% (60 minutes). As a result, the storage modulus decreased with increasing the degree of crystallinity [29].

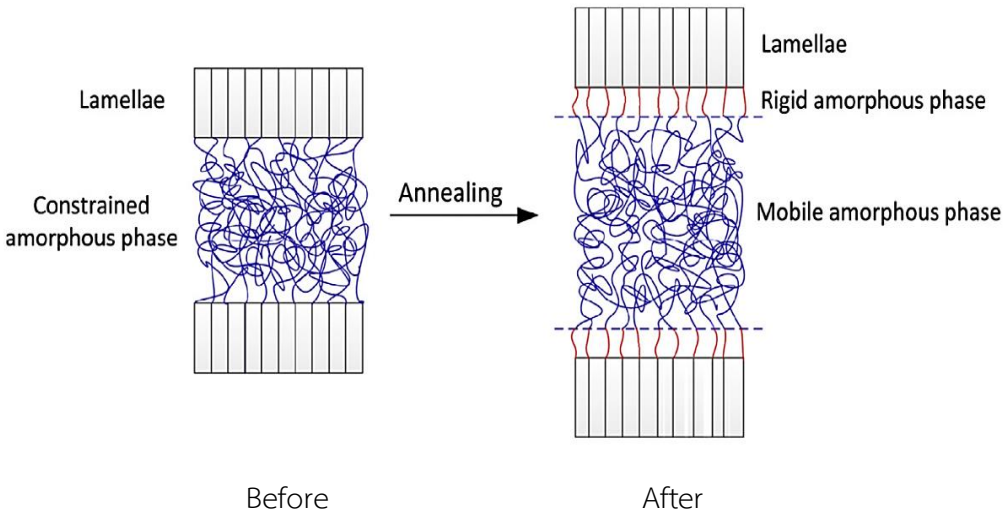

Figure 2.5 Schematic drawing of PLA samples before and after annealing at elevated temperature [26]

2.4.2 Incorporation of fillers

Generally, filler has been added into polymer to reduce cost and improve the mechanical properties of the polymer composites; however, filler is also the important factor influencing the crystallization behaviors such as crystallization kinetics, crystal structure, crystalline morphology of the polymer composites. Fillers including talc, $CaCO_3$, montmorillonite clay have been added to improve the crystallization of PLA [4, 15, 30]. Talc acted as an effective filler for accelerating the cold-crystallization rate of PLA, especially at high talc content [11]. It was shown that talc gave the two dimensional growth on an epitaxial growth [25]. Unfortunately, elongation at break and impact strength decreased due to the poor interfacial adhesion between PLA matrix and talc particles [5].

Starch is a partial crystalline polymer as a consequence of residual crystallinity and the recrystallization of amylose and amylopectin. Starch as a filler in the commodity plastics can slightly increase the crystallization rate [31, 32]. Adding starch content of 40 wt% decreased Avrami index (n) because of the nucleation density and restriction of crystalline formation due to filler concentration [31]. Non-isothermal crystallization kinetics of PP/10 wt% $CaCO_3$ reported an increased crystallization temperature (T_c) because of the enhanced interactions between the filler and PP matrix. The faster crystallization rate depended on the cooling process [33]. The addition of 10 wt% elastomer in the PLA matrix showed an increase in the cold crystallization rate constant (k) of PLA composites under isothermal condition at 90°C

from $0.104x10^{-3}$ 1/s to $0.431x10^{-3}$ 1/s [15]. The PLA composites had lower cold-crystallization half-time ($t_{1/2}$) in comparison with that of neat PLA due to the addition of filler [18].

The overall crystallization kinetics and spherulitic morphology were controlled by many factors such as bulk nucleation density, nucleation density on the filler surface, spherulitic growth rate, volume fraction and diameter of filler. At the same volume content of fibers, stronger effect was observed for thinner fibers [14]. Unfortunately, the dispersion of filler in the polymer composites was poor due to the weak interaction between fillers and polymer matrix, resulting in the agglomeration of filler. Thus, the surface modification by silanization of filler is performed in this research to improve the interfacial adhesion and mechanical properties of the polymer composites.

2.4.3 Functionality on the filler surface

Thermoplastics provide a great challenge in promoting adhesion through silane coupling agent than thermosets. Silane coupling agents are silicon-based chemicals containing two types. General structure of silane coupling agent is $(RO)_3SiCH_2CH_2CH_2$-X, where RO is a hydrolyzable group such as methoxy and ethoxy. X is an organofunctional group such as amino, vinyl and epoxy [9, 10, 34, 35]. According to previous works, for PP filled with surface-modified talc by organosilane coupling agent it was found that T_c decreased as increasing talc content because an increase in the

interactions between the silane-treated talc particles and the PP matrix, promoting faster crystallization during the cooling down process. The crystallization half-time decreased when silane-treated talc was filled in the PP matrix [36]. Moreover, the modified surface of talc with the incorporation of 3-aminopropyltriethoxy silane and Lica 12 showed that the 3-aminopropyltriethoxy silane treatment slightly reduced the crystallization kinetics of PP/30 wt% talc. On the other hand, the coupling agent, Lica 12 could improve the filler dispersion of both filler-matrix and filler-filler interactions. Further, increasing filler dispersion reduced the hindrance of the particles and allowed better spherulite growth and rearrangement [10].

The morphologies of LDPE/ 50 wt% cellulosic fibers with the surface modification by silanization were observed by a scanning electron microscope (SEM) as illustrated in Figure 2.6 [37]. The functional group of LDPE/50 wt% cellulosic fibers treated with γ-methacryloxypropyltrimethoxysilane (MPS) could increase the interfacial adhesion and no voids on the fractured surface between LDPE and cellulosic fibers phase were observed. Moreover, the mechanical properties of LDPE/50 wt% cellulosic fibers treated with MPS showed an increase in tensile strength and Young's Modulus by 26% and 17%, respectively, because functional groups can rise the chemical bonding between fibers and matrix [37]. The degree of crystallinity of PP/1 wt% modified carbon black increases from 43.3% (PP/ 1wt% carbon black) to 57.8%, which might be because the modified carbon black could reduce the particle agglomeration, leading to a more uniform dispersion of modified carbon black in PP matrix [38].

As a result, the surface modification by silanization of filler can significantly improve the interfacial adhesion, mechanical properties and the crystallization rate of the polymer composites.

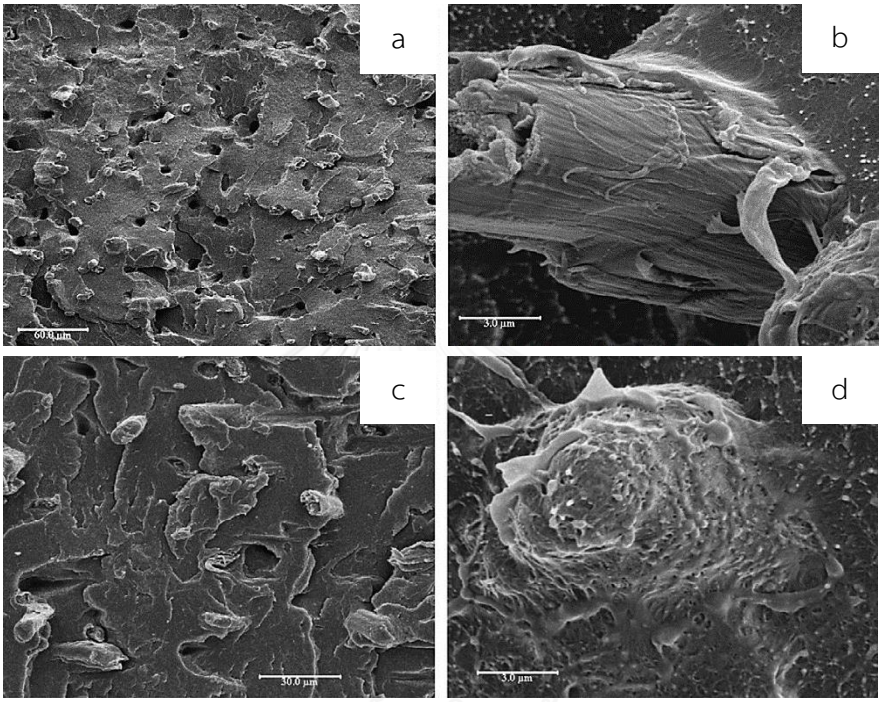

Figure 2.6 SEM images of the LDPE/50 wt% cellulosic fibers with surface modification by silanization (a,b) the LDPE/50 wt% cellulosic fibers (c,d) the LDPE/50 wt% cellulosic fibers treated with **γ**-methacryloxypropyltrimethoxysilane (MPS) [37]

CHAPTER III

EXPERIMENTS

3.1 Materials

Commercially available poly(lactic acid) (PLA) (grade 2003D) with a density of 1.24 g/mL was supplied by NatureWorks LLC, USA. The micron-sized talc with a mean particle size of 6 μm (density of 0.611 g/mL) and calcium carbonate ($CaCO_3$) with a mean particle size of 8 μm (density of 1.250 g/mL) were provided by Thai Chemical Industries, Thailand. Cassava starch with a density of 0.650 g/mL was obtained from Thai Wah Food Products Public Company Limited, Thailand.

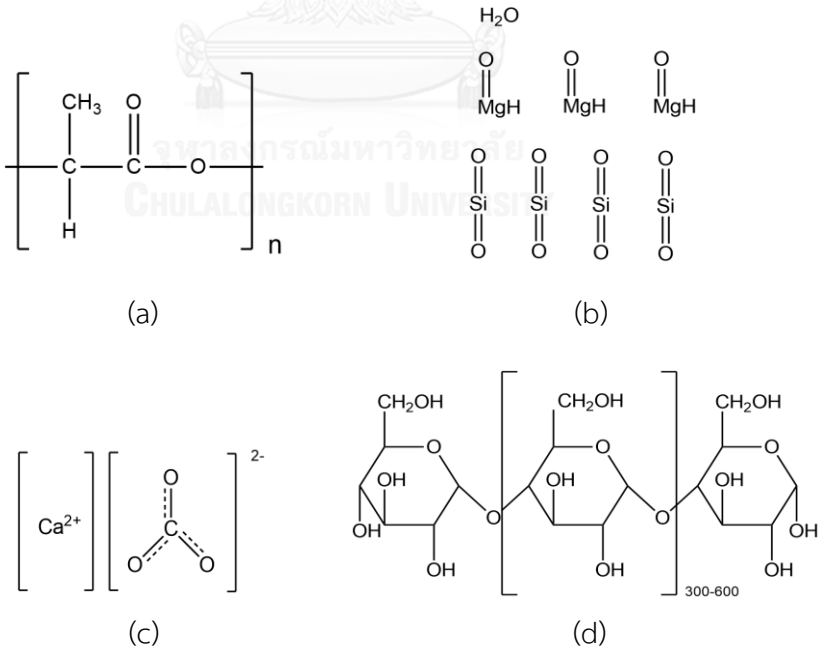

(a) (b)

(c) (d)

Figure 3.1 Chemical structures of (a) PLA, (b) talc,

(c) $CaCO_3$ and (d) cassava starch

3.2 Preparation of thermoformed PLA composites

The methodology to prepare thermoformed PLA composites containing talc, calcium carbonate and starch at different volume compositions is illustrated in Figure 3.1. Filler content was varied between 1-10 vol%. PLA pellets and fillers were predried in an oven at 60°C for 24 h to remove the moisture. Then, the composites were prepared in a co-rotating twin extruder (Labtech Engineering, Thailand, L/D=40 and D=20) with a mixing temperature between 165-180 °C and a screw speed of 50 rpm.

For the functionalization using silane coupling agent, 3-aminopropyltriethoxysilane (APTES) and vinyltriethoyxsilane (VTES) were selected. Filler was predried at 60 °C for overnight to remove the moisture. A mixture of deionized water and 1 wt% acetic acid was prepared, and the silane coupling agent was slowly dropped into the mixture until the required concentration was obtained. The silane solution was prepared in the acetic acid mixture because it was more reactive in the acidic condition. The silane solution was added into the filler. The mixing was performed at room temperature for 1 h with a magnetic stir bar. The functionalized filler was washed with distilled water several times to remove the untreated silane. Finally, filler was dried in an oven at 60°C overnight in the oven to remove the moisture.

The PLA composites were then casted into sheets by a twin screw extruder equipped with a cast-film die (Thermo Haake, Rheocord 300p and Rheomex PTW16/15 and 16/25, Germany). The processing temperature was ranged at 130-185°C and a screw speed of 80 rpm. Finally, sheets of PLA composites were thermoformed at different temperatures using a laboratory thermoforming machine with vacuum apparatus.

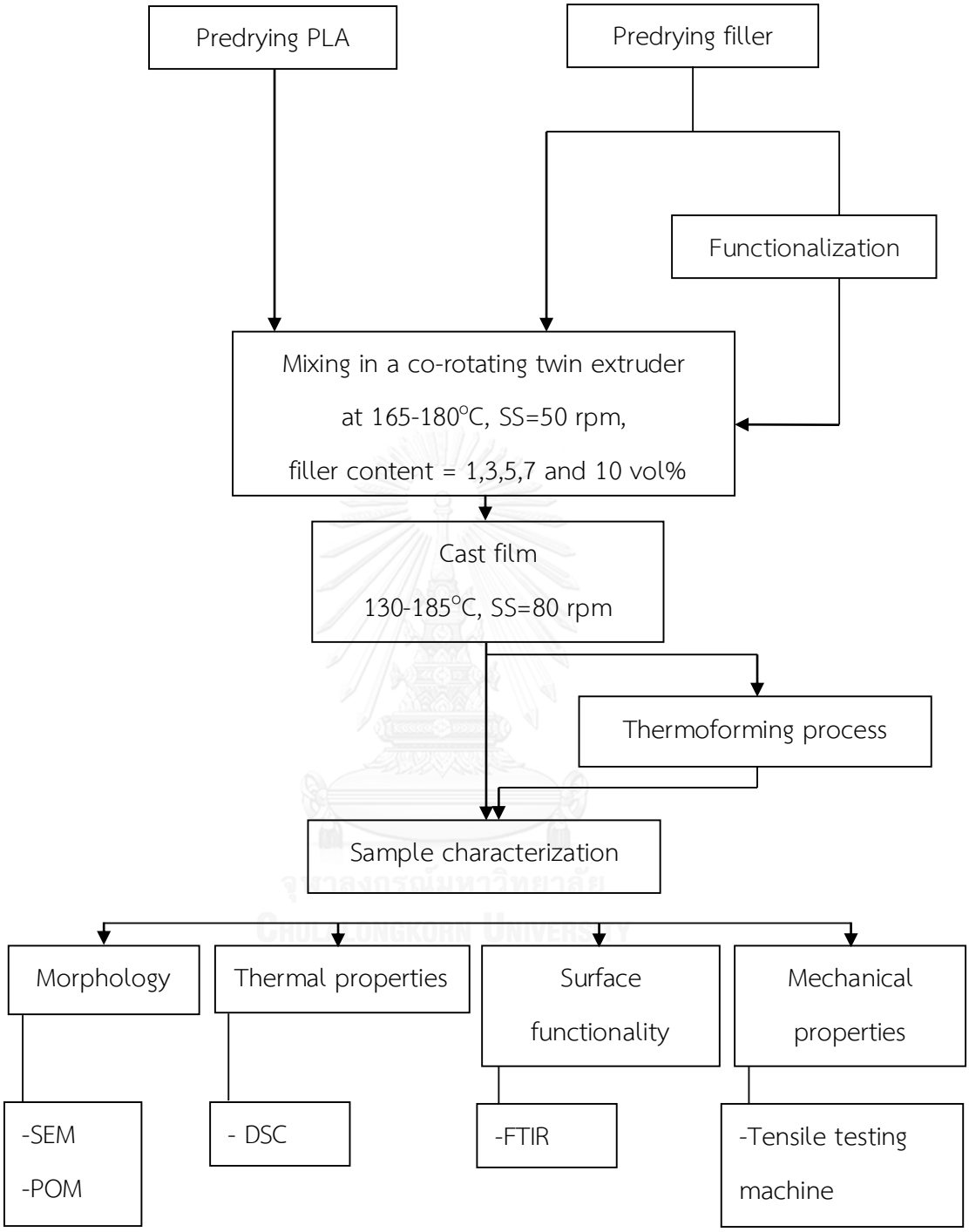

Figure 3.2 The schematic diagram of preparation and characterization of PLA composites

3.3 Sample characterization

3.3.1 Functional groups on the filler surface

Functionalization of treated filler and untreated filler was confirmed using an attenuated total-reflectance technique (ATR) in conjunction with a Fourier transform infrared (FTIR) spectroscopy (GX, Perkin-Elmer, USA). The spectrum was collected in the wavenumber ranging from 400-4000 cm^{-1} at a resolution of 4 cm^{-1} and number of scan of 100.

3.3.2 Morphology

The morphology of the cross-sectional fractured surface of neat PLA and its composites was observed by a scanning electron microscope (SEM) (JEOL, JSM- 6400, Japan) with an acceleration voltage of 8 kV. All samples were fractured in a liquid nitrogen. The sample was coated with gold to prevent the electrical discharge prior to examination. The average particle size in the composites was examined by an image analysis software.

3.3.3 Thermal properties

Thermal properties and isothermal cold-crystallization kinetics of neat PLA and its composites were measured using differential scanning calorimetry (Perkin-Elmer, Diamond DSC, USA). Approximately 5-10 mg of samples were put in an aluminum pan.

The sample was firstly heated to 190°C at the rate of 10°C/min and was held for 5 min to remove thermal history. Subsequently, the sample was cooled to 50°C at 10°C/min and reheated again to 190°C with a rate of 10°C/min. The measurement was done under N_2 purge. The crystallinity was calculated from the second heating scan.

For isothermal cold-crystallization kinetics, the sample was heated from 50°C to the determined isothermal temperature (T_c) ranged from 90, 100, 110, 120 and 130°C at the rate of 80°C/min. The development of exothermic heat flow under isothermal condition was recorded. Glass transition temperature (T_g), cold-crystallization temperature (T_{cc}) and melting temperature (T_m) were obtained from the heat flow. The degree of crystallinity (%X_c) was calculated as follows:

$$\%X_C = \frac{(\Delta H_m - \Delta H_{cc})}{(\Delta H_m^{\circ} \times \emptyset)} \times 100 \qquad (3.2)$$

Where ΔH_m and ΔH_{cc} were the enthalpies of the melting and cold crystallization of neat PLA and its composites, respectively. ΔH_m° was the melting enthalpy of 100% crystalline PLA (93 J/g). ∅ was weight fraction of PLA in the samples.

3.3.4 Growth of PLA crystals

The growth of the crystalline structure of PLA in neat PLA and its composites under isothermal cold-crystallization was measured by a polarized optical microscope (POM) (Nikon, model LV100pol, Japan) equipped with a hot stage. The sample placed between a glass slide and a cover slip at 10X (100 μm) of magnification. The sample

was heated to the isothermal temperature ranged from 90°C to 130°C at a rate of 50°C/min and was held for 40 min to observe the growth of the crystalline structure.

3.3.5 Mechanical properties

Tensile properties including of tensile strength, Young's modulus, toughness and elongation at break in MD were recorded on a universal testing machine (Intron model 5567, USA) following ASTM D882 at 12.5 mm/min of crosshead speed and 1kN of load cell. The specimen with a rectangular shape (10 mm x 100 mm) was cut from cast film sample and the thermoformed sample.

CHAPTER IV

RESULTS AND DISCUSSION

Herein, in the first part, the effect of talc, $CaCO_3$, and starch in the PLA composites on the thermal properties, tensile properties, and isothermal cold-crystallization behavior under isothermal condition at 90, 100, 110, 120 and 130°C was investigated. The parameters including isothermal temperature as well as type and content of filler from the first part that give the fastest isothermal cold-crystallization rate of the PLA composites were chosen for the second part, which is a study on the effect of chemical surface modification of filler with 3-aminopropyltriethoyxsilane (APTES) and vinyltriethoyxsilane (VTES). The properties of PLA cast films and PLA thermoforming films were examined.

4.1 Effects of filler type and filler content on the properties of the PLA composites

4.1.1 Thermal properties of PLA cast films

The thermal properties and crystallization behavior of neat PLA and PLA composites from the cast films were investigated from the second heating scan of dynamic DSC measurement. The values of glass transition temperature (T_g), cold crystallization temperature (T_{cc}), melting temperature at low temperature (T_{m1}) and

high temperature (T_{m2}), enthalpy of cold crystallization (ΔH_{cc}), enthalpy of melting (ΔH_m) and degree of crystallinity ($\%X_c$) were determined from the DSC profiles, which were tabulated in Table 4.1. It was clearly seen that the presence of filler in the PLA matrix did not affect the T_g of PLA. T_g of neat PLA and PLA composite were approximately 58°C. No shift of T_g implied that the miscibility of PLA and filler was not observed.

Considering the cold crystallization temperature (T_{cc}), talc can accelerate the cold crystallization better than $CaCO_3$, as can be confirmed by a shift of T_{cc} to lower temperature and an increase in degree of crystallinity. However, the degree of crystallinity was not enhanced when starch was incorporated. This result suggested that talc and $CaCO_3$ had the nucleating ability under non-isothermal condition where talc acted as the best nucleating agent among chosen fillers in this study. This might be due to the fact that the surface chemistry of talc effectively facilitates the cold crystallization mechanism of PLA. The effect of surface chemistry of filler on the cold crystallization behavior of PLA will be examined in the second part. Furthermore, the cold crystallization enhancement was more pronounced as a content of talc increased because more surface area for nucleation process was provided. For example, the degree of crystallinity of PLA of Talc1, Talc3, Talc5, Talc7 and Talc10 were 8.5, 9.2, 10.3, 14.5 and 15.8%, respectively, while $CaCO_3$5 had the degree of crystallinity of 9.1%. Considering the melting behavior, the double-peak melting temperatures of neat PLA and PLA composite sheets were observed by DSC

thermograms. The melting peak at higher temperature (T_{m2}) belongs to more prefect crystalline structure than that at lower temperature (T_{m1}). The crystal structure at the lower temperature is called loose crystals and that at the higher temperature is called dense crystals. The DSC thermograms of neat PLA and PLA composites from the first heating scan were illustrated in Appendix B.

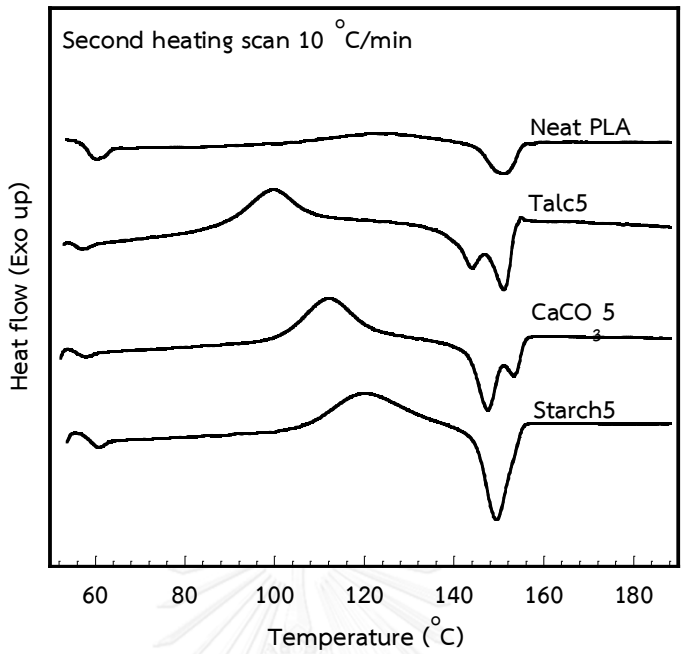

Figure 4.1 DSC thermograms of PLA-composite cast films from the second heating scan

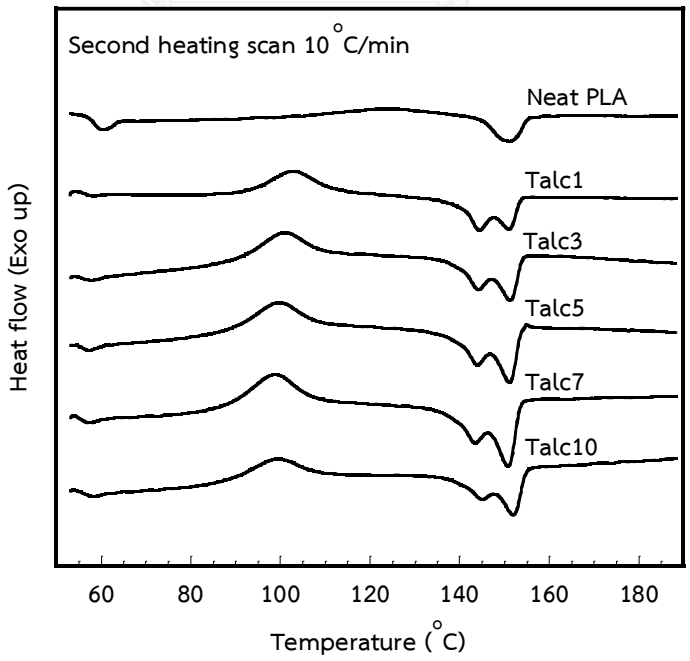

Figure 4.2 DSC thermograms of PLA/Talc cast films from the second heating scan

Table 4.1 Thermal properties of PLA composite cast film containing different types of fillers determined from the second DSC heating scan

Samples	$T_{g\ PLA}$ (°C)	T_{cc} (°C)	T_{m1} (°C)	T_{m2} (°C)	ΔH_{cc} (J/g)	ΔH_{m} (J/g)	$\%X_{c}$
Neat PLA	58.8	125.9	149.7		4.6	10.1	6.1
Talc5	58.6	99.9	143.8	151.1	19.9	29.2	10.3
$CaCO_3$5	58.7	111.9	147.6	153.7	22.1	30.1	9.1
Starch5	58.6	118.2	148.3	151.2	21.7	27.2	6.0

Table 4.2 Thermal properties of PLA/Talc cast films containing different talc contents determined from the second DSC heating scan

Samples	$T_{g\ PLA}$ (°C)	T_{cc} (°C)	T_{m1} (°C)	T_{m2} (°C)	ΔH_{cc} (J/g)	ΔH_{m} (J/g)	$\%X_{c}$
Neat PLA	58.8	125.9	149.7		4.6	10.1	6.1
Talc1	58.8	102.8	144.4	151.2	18.4	26.5	8.5
Talc3	58.5	100.5	144.1	151.2	14.4	22.7	9.2
Talc5	58.6	99.9	143.8	151.1	17.8	30.7	10.3
Talc7	58.8	98.5	143.4	152.1	17.8	30.7	14.5
Talc10	58.7	99.5	144.8	152.1	15.4	29.3	15.8

4.1.2 Isothermal cold crystallization kinetics

The effects of filler type and filler content in the PLA composites on the isothermal crystallization kinetics of PLA at isothermal temperature in a range of 90-130°C were investigated. Figure 4.4 represents the relative degree of crystallinity (X_c) versus crystallization time (t) for PLA composites at 100°C. The cold-crystallization half-time ($t_{1/2, exp}$) was defined as the time required to obtain 50% of total crystallinity from cold-crystallization process. The values of $t_{1/2, exp}$ for PLA composites at 100°C arranged the following order: Talc5 < $CaCO_3$5 < Starch5 < neat PLA. The $t_{1/2, exp}$ values at 100°C of neat PLA, Talc5, $CaCO_3$5 and Starch5 were 4.6, 2.0, 3.2 and 3.7 min, respectively. The shorter $t_{1/2, exp}$ mean the faster cold crystallization rate. Clearly, it can be seen that incorporation of talc content up to 5 vol% reduced the $t_{1/2, exp}$ values, indicating the faster cold-crystallization rate as illustrated in Figure 4.5. The result supported the effective nucleating ability of talc for isothermal cold crystallization of PLA.

Moreover, the crystallization kinetics parameters were also calculated in this work in order to describe the cold-crystallization mechanism. A theoretical Avrami model was conducted to examine the crystallization kinetics of the PLA and PLA composites. The Avrami model parameters were described in section 2.3.2. Figure 4.6 illustrates the plots of $t_{1/2, exp}$ versus crystallization temperature (T_c) for neat PLA and PLA composites. The PLA composites had the lowest $t_{1/2, exp}$ at the crystallization temperature of 100°C. At low temperature, that is 90 °C, the mobility of

PLA chains is restricted because it is closed to the glassy state ($T_{g, PLA}$ = 58 ^{o}C) and thus the rearrangement of PLA chains to form crystalline structure is difficult, leading to longer $t_{1/2, exp}$. At high temperature, that is 130 ^{o}C, the PLA chains received high thermal energy and the PLA chains favors the chain movement rather than crystallization, resulting in longer $t_{1/2, exp}$ as well. The isothermal temperature that provides fastest cold crystallization rate under isothermal condition in this study was around 100 - 110 ^{o}C.

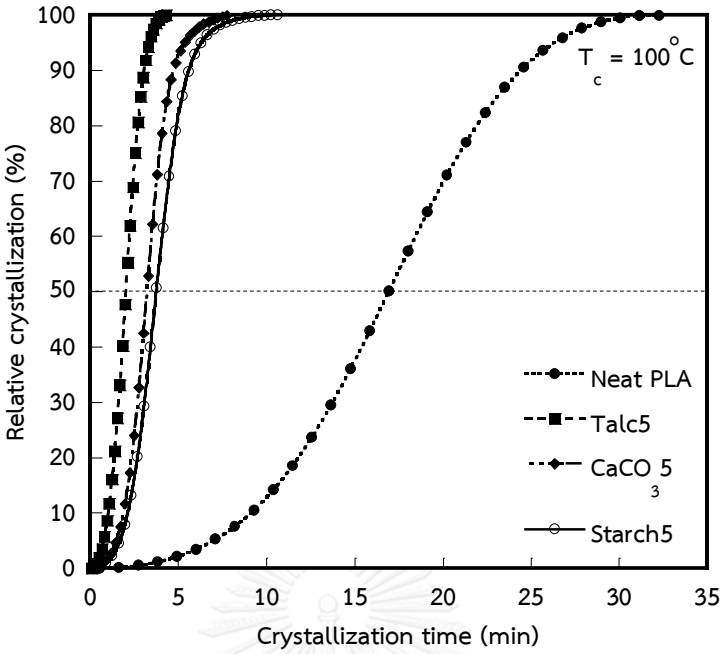

Figure 4.3 Relative degree of crystallinity (X_c) versus crystallization time (t_{exp}) for PLA/talc composites at 100°C

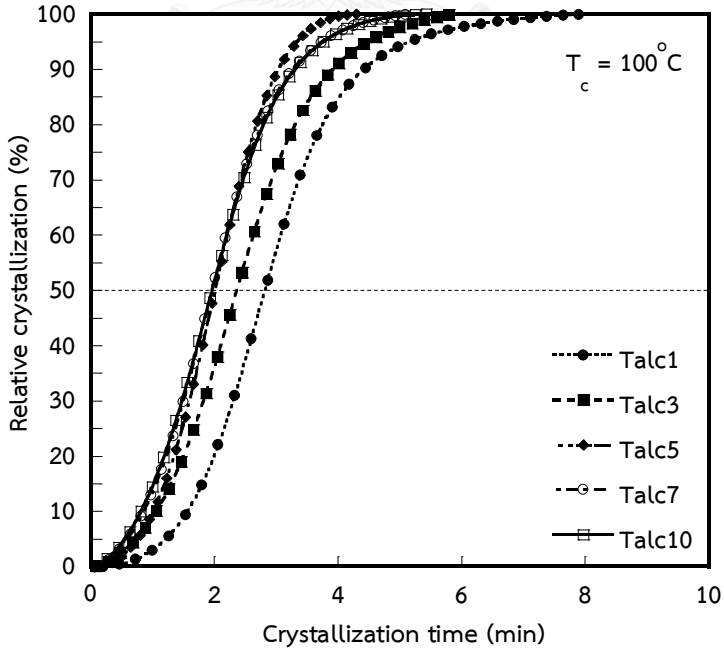

Figure 4.4 Relative degree of crystallinity (X_c) versus crystallization time (t_{exp}) for neat PLA and PLA composites at 100°C

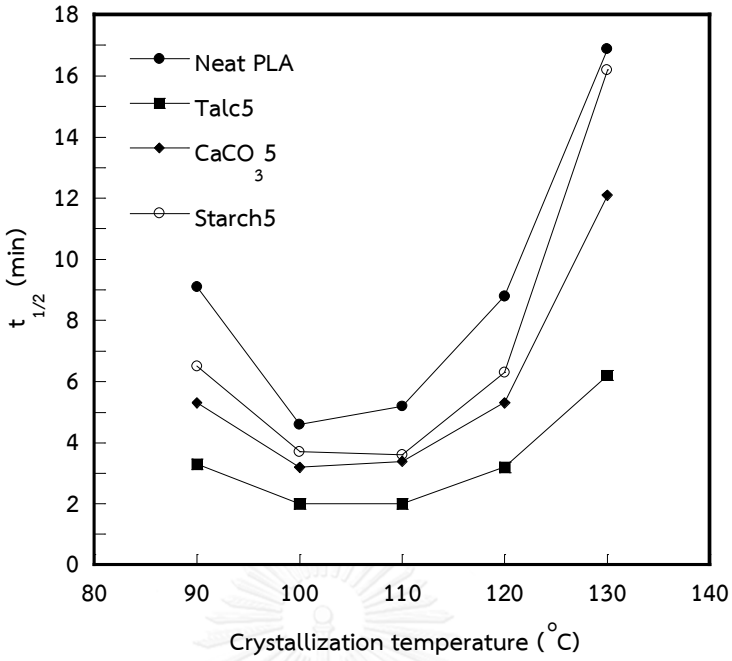

Figure 4.5 Isothermal cold-crystallization half time ($t_{1/2}$) as a function of isothermal crystallization temperature for neat PLA and PLA composites at different temperatures

The Avrami model showed the straight lines with a large coefficient of determination (R^2>99%), which refers that Avrami model can fit the experimental data pretty well for describing the isothermal cold-crystallization kinetics. The Avrami index (n) and the crystallization rate constant (k) can be examined from the slope and the y-intercept of the curve of the experimental data. Figure 4.7 represents the Avrami plots of log [-ln (1-X_c)] versus log [t (min)] for the PLA composites containing various talc contents (1-10 vol%) at 100°C. The k value increased with increasing filler content up to 5 vol%. Namely, k values of neat PLA, Talc5, $CaCO_3$5 and Starch5 were $5.43x10^{-3}$, $3.74x10^{-2}$, $8.71x10^{-3}$ and $4.50x10^{-3}$ min^{-1}, respectively.

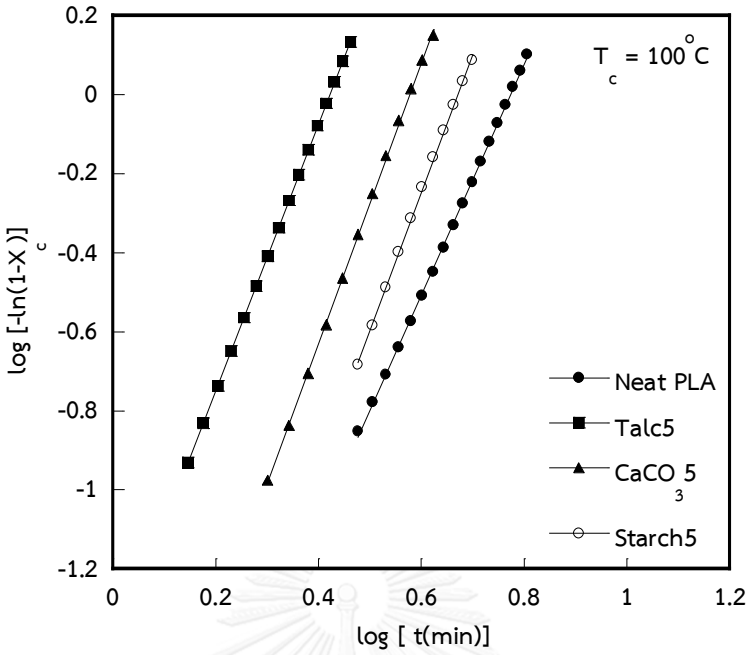

Figure 4.6 Avrami plots of log [-ln (1-X_c)] versus log t_{cal} for isothermal cold-crystallization for neat PLA and PLA composites at 100°C

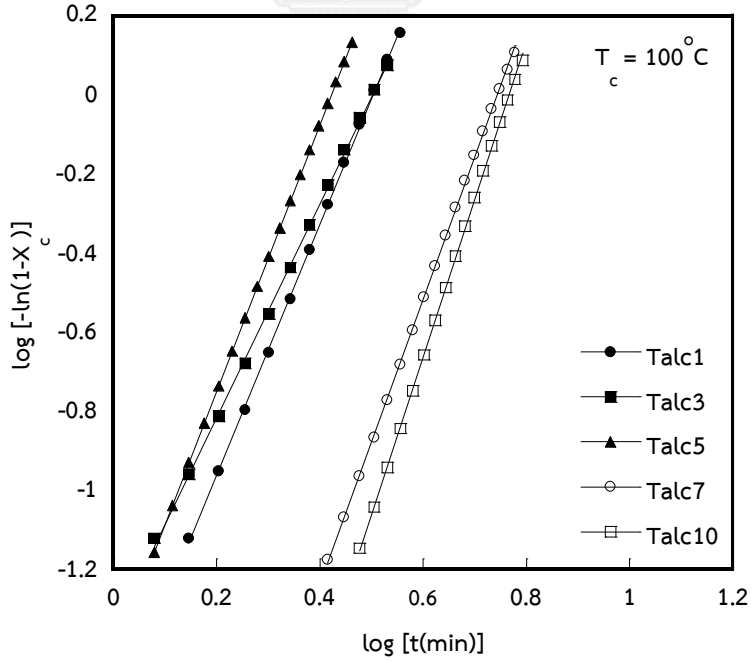

Figure 4.7 Avrami plots of log [-ln (1-X_c)] versus log t_{cal} for isothermal cold-crystallization for PLA/talc at 100°C

Table 4.3 Isothermal crystallization kinetic parameters calculated from Avrami model for neat PLA and its composites at different crystallization temperatures and filler contents.

Sample	T_c (°C)	Avrami index (n)	K (min^{-1})	$t_{1/2, exp}$ (min)	$t_{1/2, cal}$ (min)	R^2
Neat PLA	90	2.6	$1.55x10^{-3}$	9.1	10.7	0.9990
	100	2.9	$5.43x10^{-3}$	4.6	5.2	0.9995
	110	3.7	$9.30x10^{-4}$	5.2	6.0	0.9998
	120	3.9	$8.85x10^{-5}$	8.8	9.4	0.9999
	130	4.0	$1.22x10^{-5}$	16.9	24.5	0.9999
PLA/Talc	90	2.9	$5.87x10^{-3}$	4.7	5.0	0.9997
1 %vol	100	3.2	$2.52x10^{-2}$	2.8	2.8	0.9997
	110	3.5	$1.36x10^{-2}$	2.7	3.0	0.9998
	120	2.6	$1.48x10^{-2}$	4.0	4.2	0.9997
	130	2.4	$3.54x10^{-3}$	7.1	9.3	0.9994
PLA/Talc	90	2.8	$1.03x10^{-2}$	3.5	3.9	0.9995
3 %vol	100	2.4	$6.86x10^{-2}$	2.3	2.5	0.9993
	110	3.2	$2.53x10^{-2}$	2.5	2.8	0.9995
	120	2.3	$3.74x10^{-2}$	3.2	3.5	0.9999
	130	2.3	$7.01x10^{-2}$	7.2	7.6	1.0000
PLA/Talc	90	2.8	$3.40x10^{-2}$	3.3	3.3	0.9983
5 %vol	100	3.4	$3.74x10^{-2}$	2.0	2.3	1.0000
	110	3.3	$2.35x10^{-2}$	2.0	2.8	0.9990
	120	2.9	$2.71x10^{-2}$	3.2	3.5	0.9998
	130	2.3	$8.56x10^{-3}$	6.2	6.7	0.9999

Sample	T_c (°C)	Avrami index (n)	K (min^{-1})	$t_{1/2, exp}$ (min)	$t_{1/2, cal}$ (min)	R^2
PLA/Talc	90	2.3	$3.24x10^{-2}$	3.6	3.7	0.9996
7 %vol	100	2.7	$6.78x10^{-2}$	2.0	2.3	0.9998
	110	2.5	$6.01x10^{-2}$	2.2	2.6	0.9994
	120	2.2	$4.73x10^{-2}$	3.1	3.4	0.9998
	130	2.0	$1.21x10^{-2}$	7.0	7.3	0.9999
PLA/Talc	90	2.4	$1.77x10^{-2}$	3.8	4.5	0.9999
10 %vol	100	2.5	$8.16x10^{-2}$	2.0	2.3	0.9999
	110	2.8	$9.99x10^{-2}$	1.8	2.2	0.9997
	120	2.2	$4.83x10^{-2}$	2.9	3.4	0.9998
	130	2.0	$1.83x10^{-2}$	6.0	6.6	1.0000
PLA/$CaCO_3$	90	3.2	$2.70x10^{-3}$	5.3	5.5	0.9998
5 %vol	100	3.6	$8.71x10^{-3}$	3.2	3.3	0.9998
	110	3.7	$3.95x10^{-3}$	3.4	4.0	0.9998
	120	3.8	$6.56x10^{-4}$	5.3	6.2	0.9998
	130	3.1	$2.12x10^{-4}$	12.1	13.2	0.9997
PLA/Starch	90	3.4	$8.90x10^{-4}$	6.5	7.1	0.9999
5 %vol	100	3.5	$4.50x10^{-3}$	3.7	4.2	0.9997
	110	3.9	$1.76x10^{-3}$	3.6	4.4	0.9998
	120	4.5	$9.13x10^{-5}$	6.3	7.2	0.9996
	130	3.8	$9.29x10^{-6}$	16.2	15.7	0.9997

The transition temperature for PLA/talc was at T_c = 100°C. The Avrami index (n) at 100°C for PLA composites was around 3.0, indicating the three-dimensional crystal growth of PLA. The crystallization parameters k, n, $t_{1/2, exp}$ and $t_{1/2, cal}$ for neat PLA and PLA composites are summarized in Table 4.3.

4.1.3 Crystalline structure of PLA under isothermal condition

Crystalline morphology for neat PLA and Talc5 was examined by a polarized optical microscope (POM). It can be clearly observed that the number and size of spherulites gradually increased as increasing crystallization time [16] Figure 4.8 (a-c) represents POM micrographs of neat PLA during isothermal crystallization at 90, 100 and 130°C. The results showed that crystallization temperature of neat PLA affected size of spherulites of PLA. For example, a small number of PLA nuclei formed and the growth rate of PLA spherulites was very slow at 130°C, whereas a dense nucleation density and fast growth rate of PLA were detected when the isothermal temperature reduced to 100°C and 90°C, respectively. Nevertheless, the number of nuclei of Talc5 was higher than that of neat PLA, indicating higher number of spherulites. As displayed in Figure 4.8 (d-f), it was observed that the nucleation density of Talc5 was higher than those of neat PLA because talc provided additional surface for PLA chains to nucleate. The result supported the effective nucleating ability of talc.

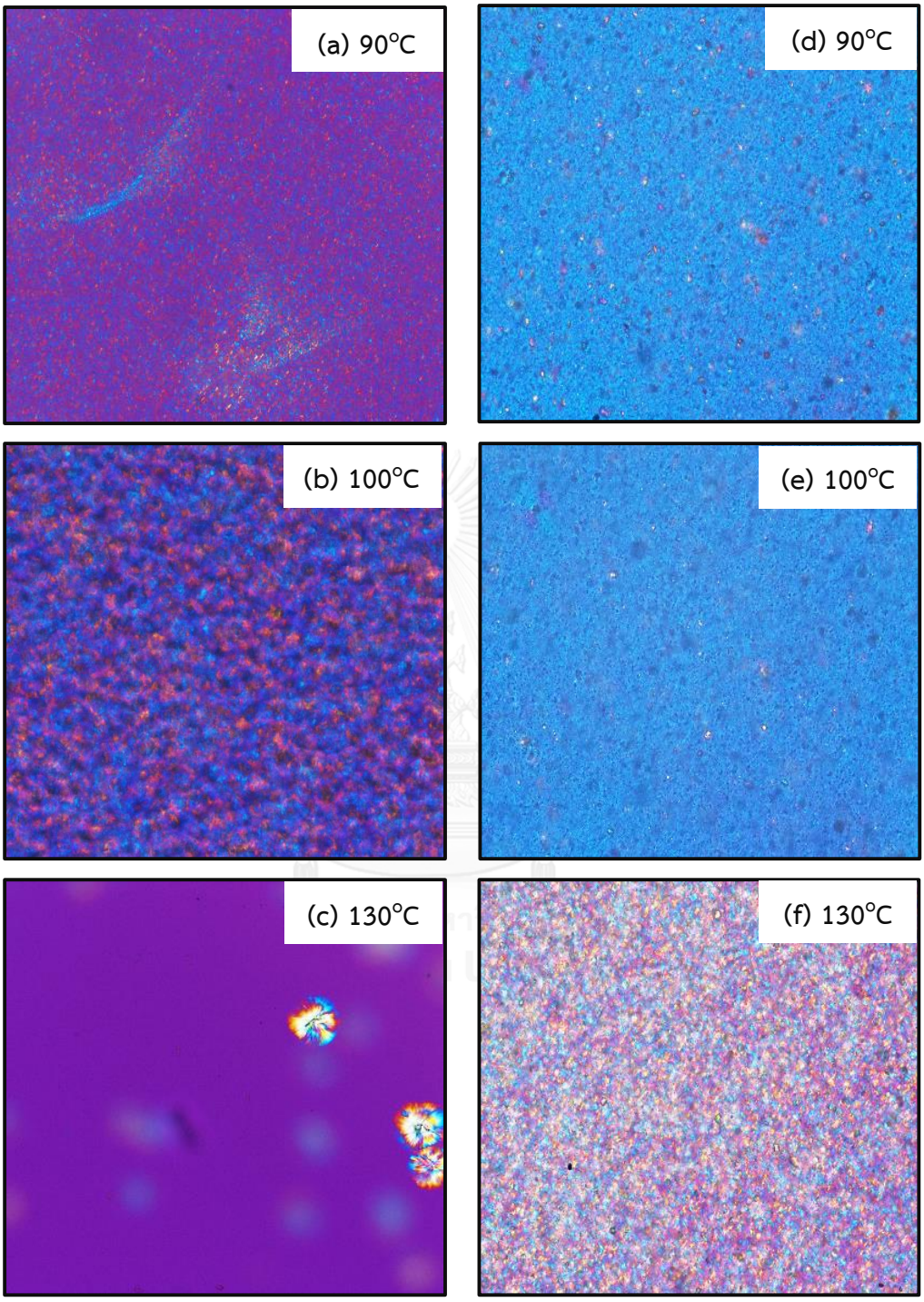

Figure 4.8 POM micrographs of spherulites of (a-c) neat PLA and (d-f) Talc5 from isothermal crystallization at crystallization temperature of 90, 100 and 130°C

4.1.4 Morphology

The crystallization rate of PLA composites depends on material properties, phase morphology and processing conditions. Appearance of cast-film PLA composites of Talc and $CaCO_3$ has smooth surface, while those of starch is slightly rough due to different characteristics of filler. Talc and $CaCO_3$ are the natural inorganic material where starch is organic one, which has less orderliness on the surface. Talc and $CaCO_3$ has more surface area than starch resulting in higher degree of crystallinity of polymer composites. Moreover, surface area was enhanced as increasing crystallization rate. The cross-sectional fractured surfaces of neat PLA and PLA composites with talc, $CaCO_3$ and starch at 5 vol% were investigated by SEM as illustrated in Figure 4.9. The SEM micrographs of (b) Talc5 exhibited the uniform dispersion of talc in the composites. There were no aggregates, whereas there were voids at the interface between talc and PLA matrix, which might indicate the poor interfacial interaction between filler and polymer matrix. Figure 4.9 (c) $CaCO_3$ demonstrated that $CaCO_3$ was pull out from the matrix due to the unwetted $CaCO_3$ in PLA. Figure 4.9 (d) Starch also showed holes and cavities at the interface between starch and PLA matrix.

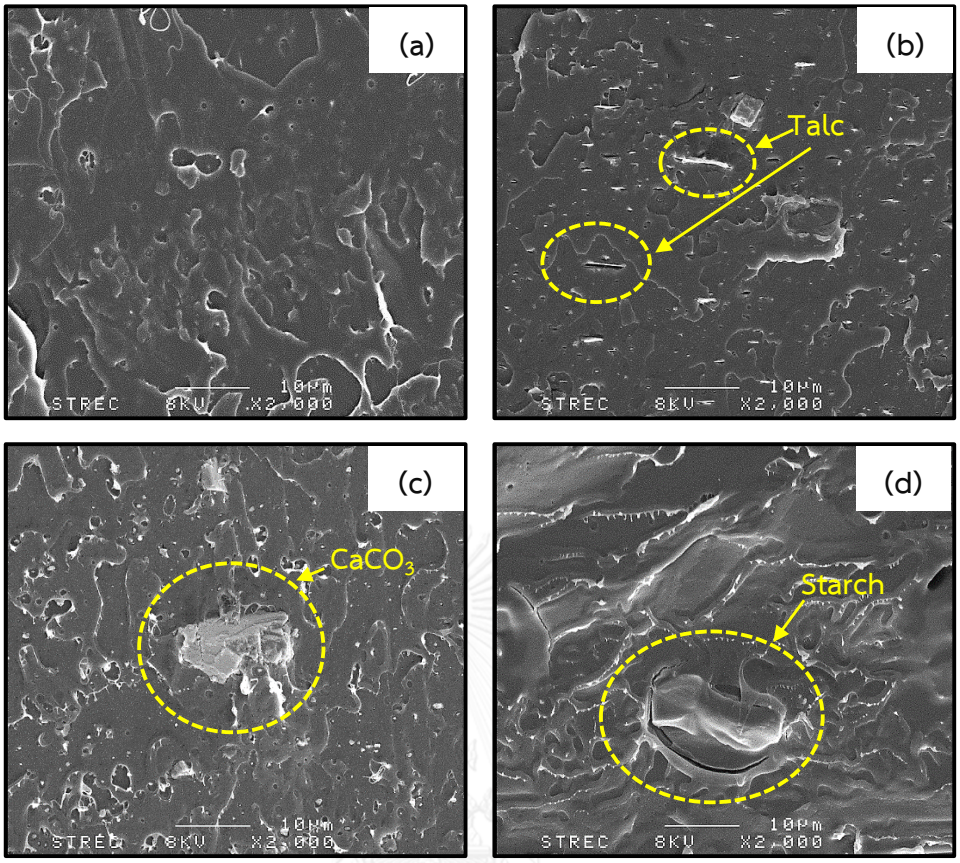

Figure 4.9 SEM micrographs of cross-sectional fractured surfaces of

(a) Neat PLA, (b) Talc5, (c) $CaCO_3$5 and (d) Starch5

4.1.5 Mechanical properties

The tensile properties of PLA cast films and PLA thermoforming films for neat PLA and PLA composites are shown in Figure 4.10-4.13 and the stress-strain curves were shown in Appendix D.1-D.2. The tensile strength at break and Young's modulus of PLA and PLA composites at 5 vol% are shown in Figure 4.10 and Figure 4.11, respectively. The tensile strength of Talc5 and $CaCO_3$5 was higher than those of neat PLA, whereas Starch5 showed lower tensile strength. This result related to the degree of crystallinity described in section 4.1.1. The degree of crystallinity of Talc5 and $CaCO_3$5 films were higher than that of neat PLA, resulting in higher rigidity of the composites. On the other hand, starch did not affect the degree of crystallinity causing no change in the value of tensile strength. The Young's modulus showed the same trend as tensile strength as can be described by the same explanation.

Both tensile strength and Young's modulus of thermoformed samples were higher than those of PLA composite cast films. There were no effect from drawing process on the sample from thermoforming process due to a use of sample from the bottom of the mold. Therefore, the reason in this case was the restriction of the chain alignment owing to increased crystallinity.[5] As a consequence, elongation at break and tensile toughness reduced, as shown in Figure 4.12-4.13. It should be noted prior to going to the next section that talc at 5 vol% provided the fastest isothermal crystallization rate of PLA, as confirmed by DSC. Since each filler showed insignificant

effect on the tensile properties, the tensile properties will not be considered in the selection of best filler type and content. In section 4.2, talc surface will be functionalized with silane coupling agents in order to study the influence of surface chemistry on the thermal and mechanical properties as well as isothermal cold crystallization of PLA composites.

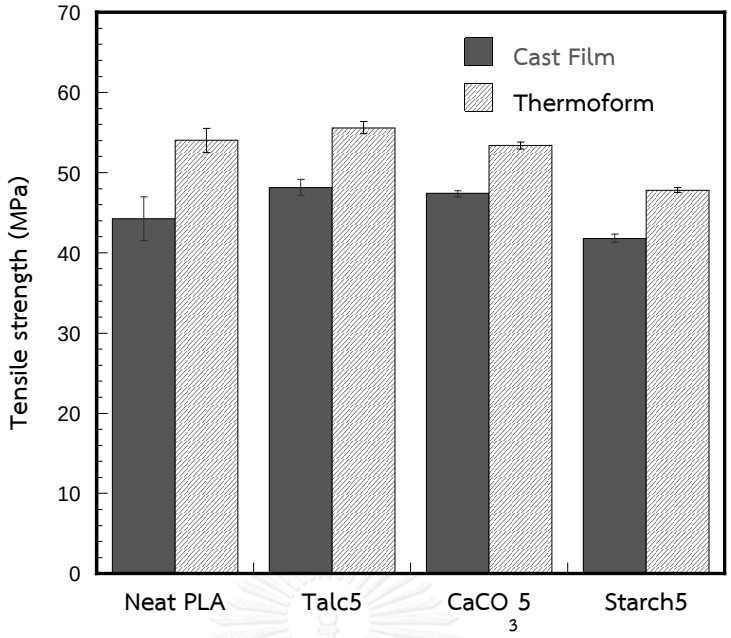

Figure 4.10 Tensile strength at break of PLA and PLA composites of PLA cast films and PLA thermoforming films

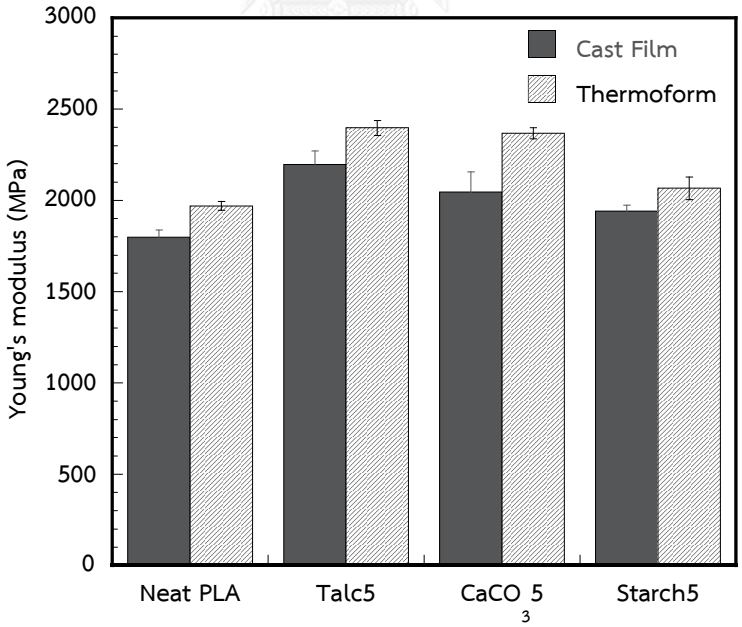

Figure 4.11 Young's Modulus of PLA and PLA composites of PLA cast films and PLA thermoforming films

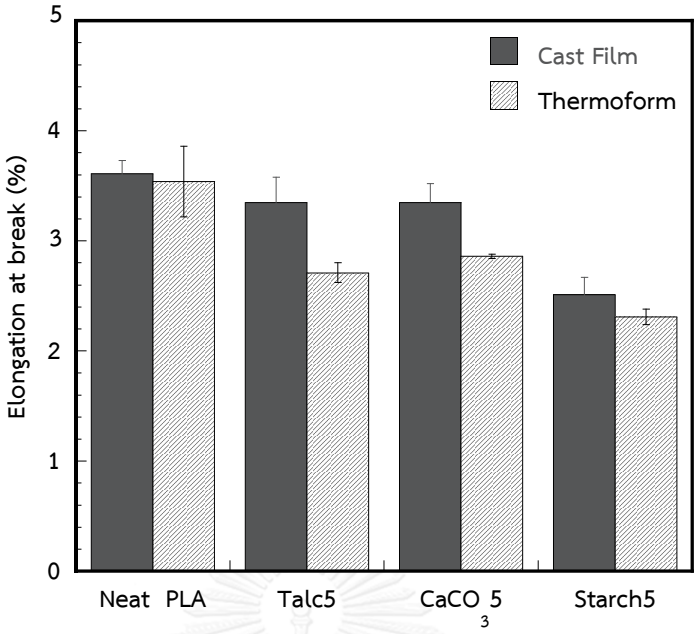

Figure 4.12 Elongation at break of PLA and PLA composites of PLA cast films and PLA thermoforming films

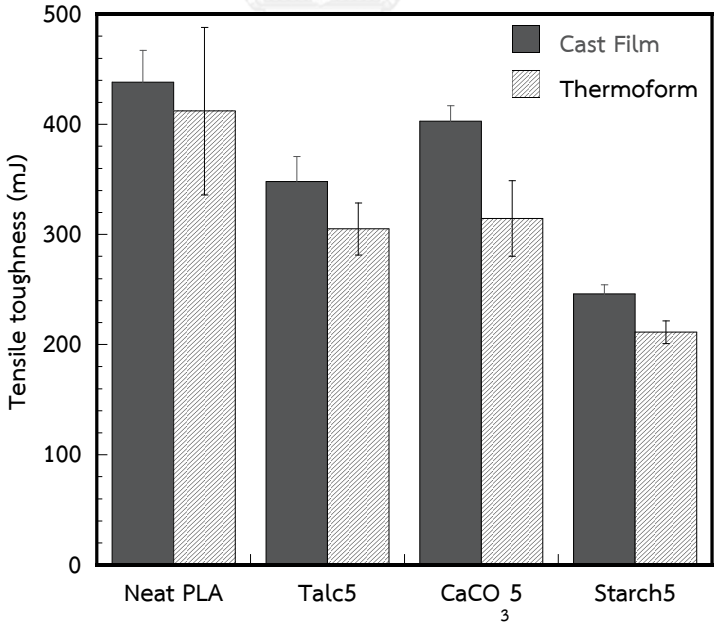

Figure 4.13 Tensile toughness of PLA and PLA composites of PLA cast films and PLA thermoforming films

4.2 Effect of chemical surface modification of filler with 3-aminopropyltri-ethoyxsilane (APTES) and vinyltriethoyxsilane (VTES)

4.2.1 Characterization of functional group on the filler surface

The surface chemistry of talc treated with 3-aminopropyltriethoyxsilane (APTES) and vinyltriethoyxsilane (VTES) were examined using FTIR spectroscopy. Silanization of talc was expected to improve the interaction between filler and PLA matrix. Figure 4.14 represents FTIR absorption spectrum of untreated talc, APTES and talc treated with APTES. The characteristic absorption bands of untreated talc at 3673.4, 1739.7, 1219.1 and 981.4 cm^{-1} belonged to the stretching of O-H, C=O, anti-symmetrical and symmetrical stretching of C-O, respectively. Furthermore, the spectrum of talc treated with APTES showed the dominant absorption peak at 1040.1 cm^{-1} and 1126.8 cm^{-1} associated to the stretching vibration of Si-O-Si and the bending vibration Si-O-Si bonds, respectively. The functional groups of talc, VTES and talc treated with VTES are shown in Figure 4.15. The absorption frequency of talc treated with VTES showed Si-O-Si and Si-O-Si bonds at 1038.1 and 1126.6 cm^{-1}, suggesting that the silane coupling agent was successfully grafted on the talc surface in spite of the fact that treated talc was purified by washing technique many times to ensure that the unreacted silane coupling agent was totally removed. The FTIR results were complementary with the SEM micrographs.

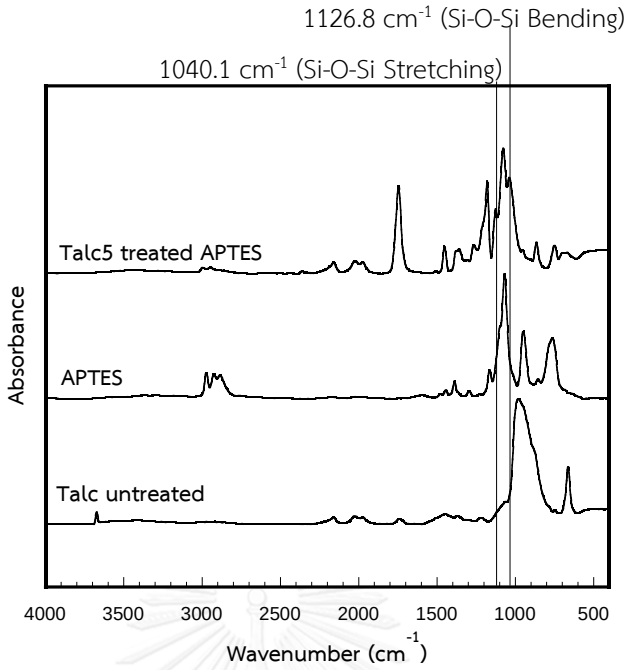

Figure 4.14 FTIR absorption spectra of untreated talc, APTES and talc treated with APTES

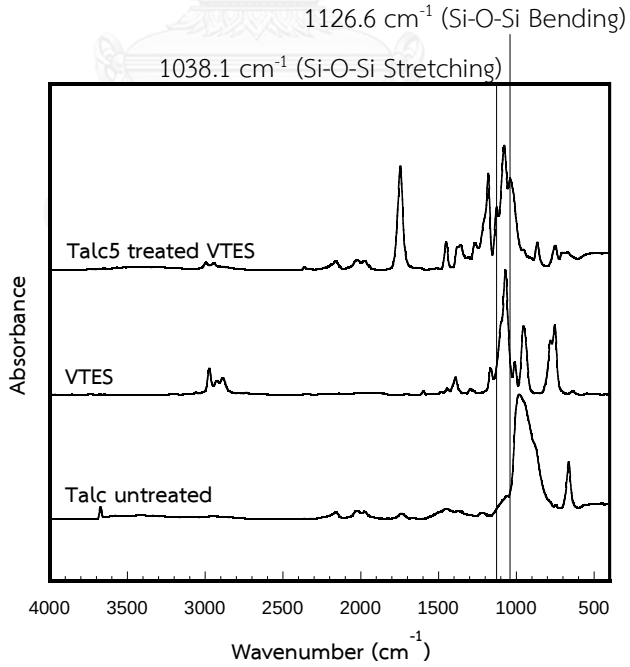

Figure 4.15 FTIR absorption spectra of untreated talc, VTES and talc treated with VTES

4.2.2 Morphology

SEM micrographs of the cross-sectional fractured surface of PLA composites with untreated and treated talc are shown in Figure 4.16. In particular, the micrograph of untreated Talc5 (Figure 4.16(a)) indicated the poor interfacial adhesion between talc and PLA matrix and voids were more obvious than the composites treated by silane coupling agent. It implied that silane coupling agent on the surface of talc improved the interaction at the interfaces between filler and polymer. Talc has the weak interlayer interaction between the lamellar platelets which are only held together by Van der Waals' force. The silane treatment can improve the interaction between filler and polymer. Namely, APTES has –NH2 which shows hydrogen bonding with the –OH and –COOH terminal groups of PLA. Besides, the similar affinity of vinyl group of VTES and PLA, leading to the enhanced wettability of treated talc around PLA chains. As a result, APTES and VTES-treated talc improved the interaction between talc particles, resulting in better dispersion of talc particles in the PLA matrix. [11]

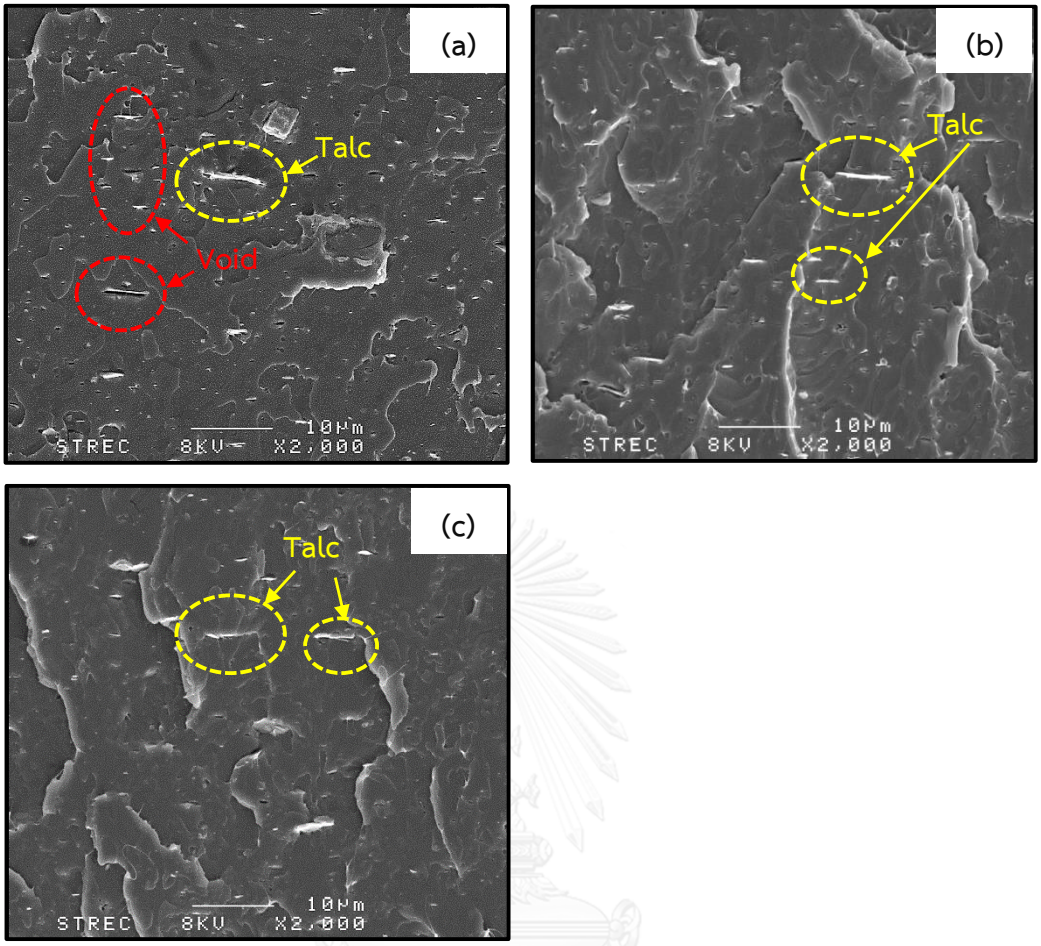

Figure 4.16 SEM micrographs of cross-sectional fractured surfaces of

(a) untreated Talc5, (b) APTES-Talc5, and (c) VTES-Talc5

4.2.3 Thermal properties

In order to investigate the thermal properties, isothermal crystallization behavior and dynamic DSC measurements were performed. DSC thermographs of composite with untreated and treated talc by APTES and VTES are demonstrated in Figure 4.17. The values of cold crystallization temperature (T_{cc}), melting temperature at lower temperature (T_{m1}) and high temperature (T_{m2}), enthalpy of cold crystallization (ΔH_{cc}), and degree of crystallinity ($\%X_c$) determined from DSC profiles are tabulated in Table 4.4. It was found that thermal properties of PLA composites significantly affected by the silane coupling agents. T_{cc} of APTES-Talc5 and VTES-Talc5 were lower than that of untreated Talc5, suggesting that silane coupling agent can accelerate the cold crystallization of PLA. The T_{cc} of untreated Talc5, APTES-Talc5 and VTES-Talc5 were 99.9, 102.76 and 98.79°C, respectively.

The enthalpy of cold crystallization (ΔH_{cc}) of APTES-Talc5 and VTES-Talc5 increased the latent energy for converting the remaining amorphous structure from crystallization condition to crystalline structure. On the contrary, the enthalpy of melting was higher than that of untreated Talc5, referring that the addition of talc treated with APTES and VTES increased the degree of crystallization. Moreover, the addition of talc treated with APTES and VTES slightly increased the degree of crystallinity due to the improvement of filler dispersion that improved the chain mobility for crystalline development.

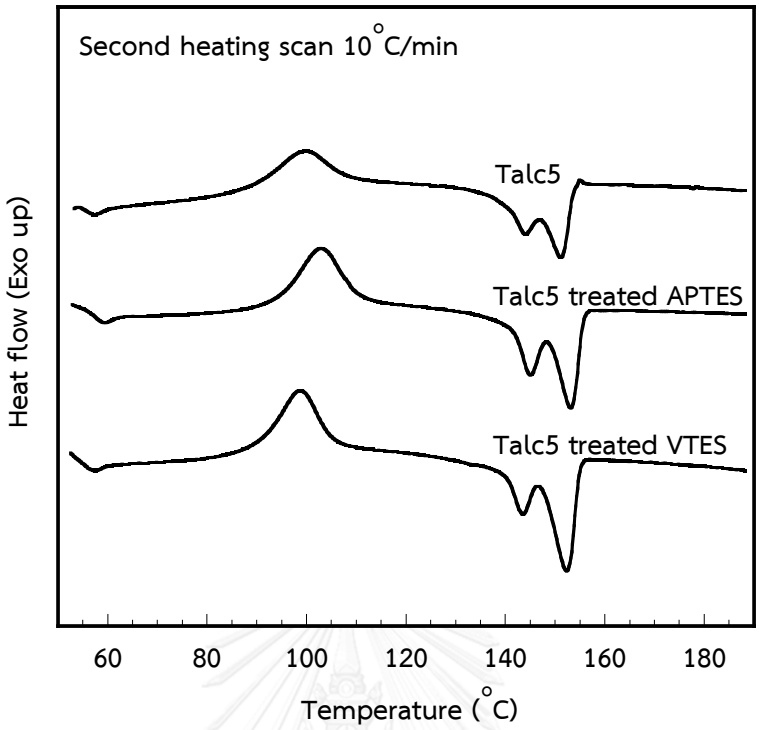

Figure 4.17 DSC thermograms of untreated Talc5, APTES-Talc5 and VTES-Talc5 from the second heating scan

Table 4.4 Thermal properties of untreated Talc5, APTES-Talc5 and VTES-Talc5 cast films from the second DSC heating scan

Sample	$T_{g\ PLA}$ (°C)	T_{cc} (°C)	T_{m1} (°C)	T_{m2} (°C)	ΔH_{cc} (J/g)	ΔH_m (J/g)	$\%X_c$
Untreated Talc5	58.6	99.9	143.8	151.1	19.9	29.2	10.3
APTES-Talc5	58.4	102.7	145.0	153.2	22.6	33.7	12.3
VTES-Talc5	58.6	98.8	143.4	152.3	21.4	33.1	12.9

4.2.4 Isothermal cold-crystallization kinetics

The addition of talc treated with APTES and VTES into PLA matrix is investigated in terms of half-time for crystallization under isothermal condition at temperature of 100°C. Clearly, Figure 4.18 shows the relative degree of crystallinity (X_c) versus crystallization time (t) in the experimental data for non-isothermal crystallization rate. It was found that surface treatment of talc gives faster crystallization rate as can be noticed by a reduction of $t_{1/2, exp}$. From SEM micrographs, sample containing treated talc shows no gap at the interface, which indicated good interfacial adhesion. The crystallization rate constant (k) values for sample composed of untreated talc, and talc treated with APTES and VTES are $3.74x10^{-2}$, $5.93x10^{-2}$ and $7.82x10^{-2}$ min^{-1}, respectively as shown in Table 4.5. Moreover, the graph of log [-ln (1-X_c)] versus log [t_{cal} (min)] for treated-talc represents the half time $t_{1/2, cal}$ were gradually increased in the value of 2.3, 1.9 and 1.9 min of untreated and talc treated with APTES and VTES as displayed in Figure 4.19. This result suggested that the enhanced interfacial adhesion does not significantly affect the crystallization rate.

Nevertheless, the Avrami index (n) at 100°C for talc treated with APTES and VTES is around 3.0, indicating the three-dimension crystallization growth in homogenous nucleation mechanism. Isothermal cold-crystallization results are complementary with the Avrami model. Besides, the crystallization rate increases due to better interfacial area.

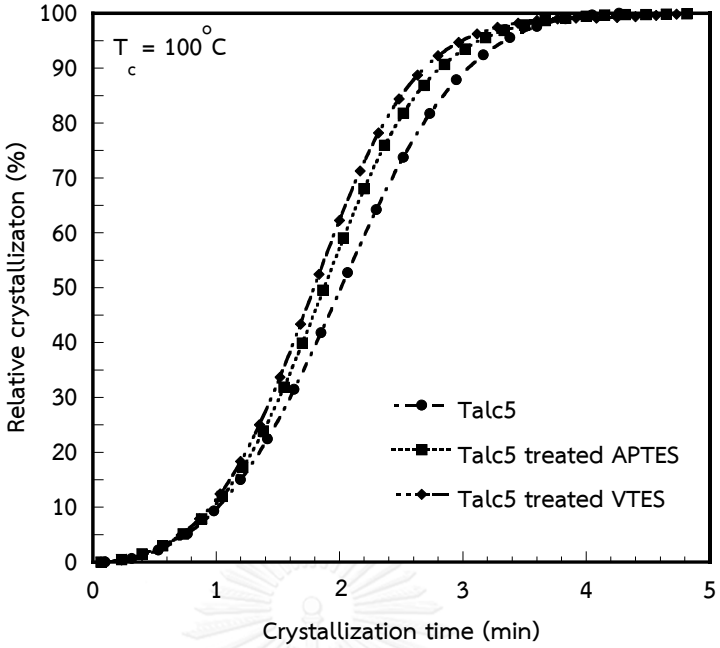

Figure 4.18 Relative degree of crystallinity (Xc) versus crystallization time (t) for untreated Talc5, APTES-Talc5 and VTES-Talc5 films at 100°C

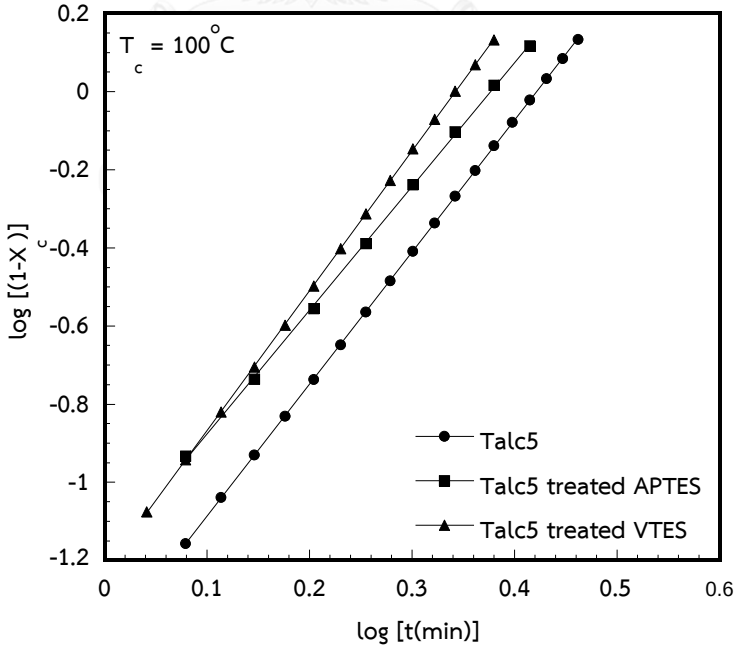

Figure 4.19 Avrami plots of log [-ln (1-Xc)] versus log t_{cal} for isothermal cold-crystallization for untreated Talc5, APTES-Talc5 and VTES-Talc5 films at 100°C

Table 4.5 Isothermal crystallization kinetic parameters calculated from Avrami model for untreated Talc5, APTES-Talc5 and VTES-Talc5 films at crystallization temperature of 100°C.

Sample	T_c (°C)	Avrami index (n)	K (min^{-1})	$t_{1/2, exp}$ (min)	$t_{1/2, cal}$ (min)	R^2
Untreated Talc5	100	3.4	$3.74x10^{-2}$	2.0	2.3	1.000
APTES-Talc5	100	3.2	$5.93x10^{-2}$	1.9	1.9	0.9997
VTES-Talc5	100	3.6	$7.82x10^{-2}$	1.9	1.9	1.000

4.2.5 Tensile properties

The tensile properties of both cast film extrusion and thermoforming process of untreated and treated talc with APTES and VTES are shown in Figure 4.20-4.23 and the stress-strain curves were shown in Appendix D.3-D.4. Tensile strength, Young's modulus, elongation at break and tensile toughness of untreated Talc5, APTES-Talc5, and VTES-Talc5 are not different, implying that enhanced interfacial adhesion does not significantly affect the load transfer much upon film stretching. However, all thermoformed films show higher stiffness (higher tensile strength and lower elongation at break) than casted film. This is because thermoforming process provides the addition PLA spherulites formation owing to the crystallization upon annealing at 100 °C.

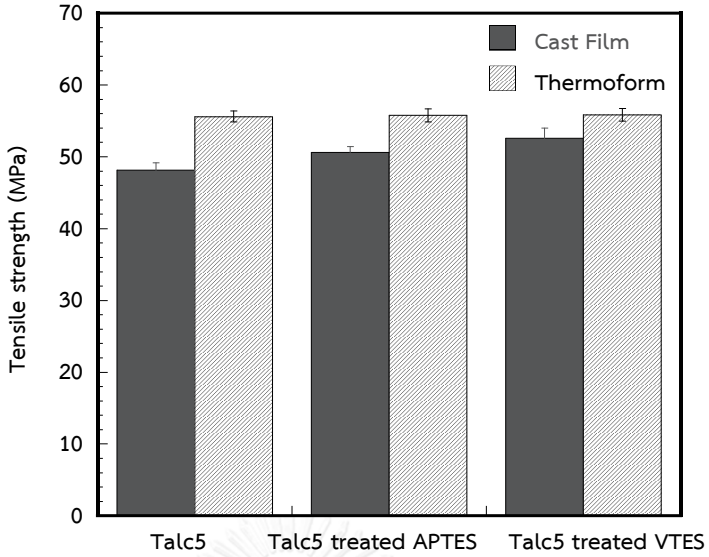

Figure 4.20 Tensile strength at break of untreated and treated Talc5 of PLA cast films and PLA thermoforming films

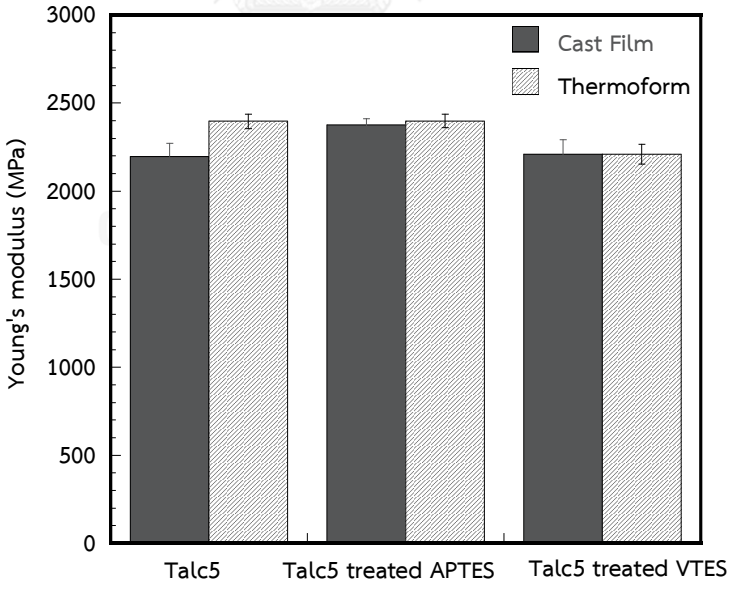

Figure 4.21 Young's modulus of untreated and treated talc5 of PLA cast films and PLA thermoforming films

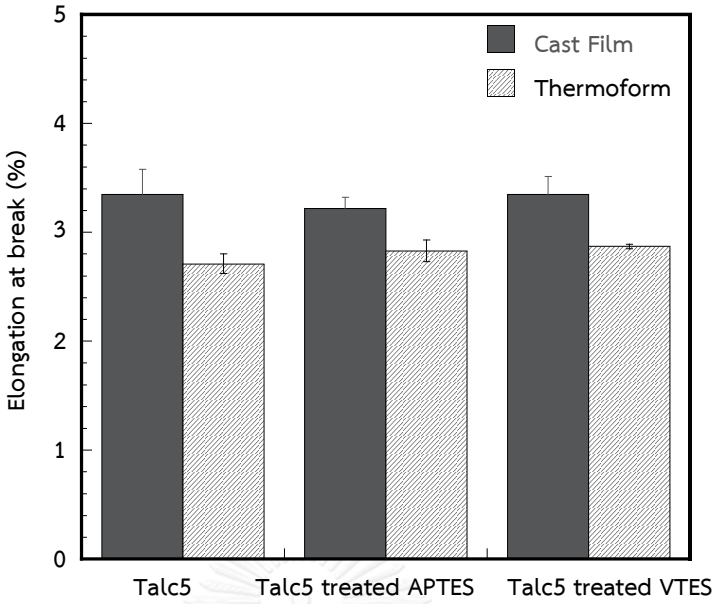

Figure 4.22 Elongation at break of untreated and treated talc5 of PLA cast films and PLA thermoforming films

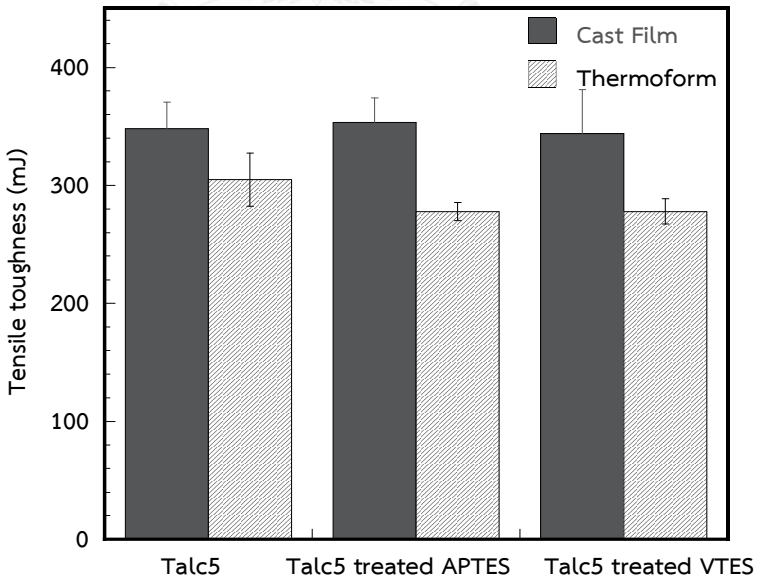

Figure 4.23 Tensile toughness of untreated and treated talc5 of PLA cast films and PLA thermoforming films

CHAPTER V

CONCLUSIONS AND RECOMMENDATIONS

5.1 Conclusions

This research aimed to improve the crystallization rate of PLA by an addition of filler and surface treatment of filler by silanization. In this study, the SEM result showed the poor interfacial interaction of filler and polymer matrix. In addition, the thermal properties confirmed the immiscibility of PLA and PLA composites as T_g did not change when adding filler. Nevertheless, the PLA composites revealed the accelerated crystallization rate of PLA as evidenced by the shortened crystallization half-time ($t_{1/2,\ exp}$) and higher crystallization rate constant (k). It was found that the crystallization rate depended on the effective nucleating ability of filler, filler content and isothermal crystallization temperature. The Avrami index (n) of all samples was around 3.0, indicating the three-dimensional crystal growth of PLA.

The interaction at the interfaces between talc and polymer was improved by silane coupling agent on the surface of talc. From the morphology result, it was indicated that the composites treated by silane coupling agent induced interfacial adhesion, comparing with the untreated talc. Moreover, the surface treatment of talc gave faster crystallization rate as can be noticed by a reduction of $t_{1/2,exp}$.

5.2 Recommendations

- Other types of silane coupling agent should be studied because the adhesion promotion of silane coupling agent could affect the crystallization rate.

REFERENCES

[1] Ke, T. and Sun, X. Melting behavior and crystallization kinetics of starch and poly (lactic acid) composites. Journal of Applied Polymer Science 89(5) (2003): 1203-1210.

[2] Zhang, J.-F. and Sun, X. Mechanical properties of poly (lactic acid)/starch composites compatibilized by maleic anhydride. Biomacromolecules 5(4) (2004): 1446-1451.

[3] Ohkita, T. and Lee, S.-H. Thermal degradation and biodegradability of poly (lactic acid)/corn starch biocomposites. Journal of Applied Polymer Science 100(4) (2006): 3009-3017.

[4] Suksut, B. and Deeprasertkul, C. Effect of Nucleating Agents on Physical Properties of Poly(lactic acid) and Its Blend with Natural Rubber. Journal of Polymers and the Environment 19(1) (2010): 288-296.

[5] Petchwattana, N., Covavisaruch, S., and Petthai, S. Influence of talc particle size and content on crystallization behavior, mechanical properties and morphology of poly(lactic acid). Polymer Bulletin 71(8) (2014): 1947-1959.

[6] Supaphol, P. and Spruiell, J.E. Isothermal melt- and cold-crystallization kinetics and subsequent melting behavior in syndiotactic polypropylene: a differential scanning calorimetry study. Polymer 42(2) (2001): 699-712.

[7] Lee, S.-H., Wang, S., and Teramoto, Y. Isothermal crystallization behavior of hybrid biocomposite consisting of regenerated cellulose fiber, clay, and poly(lactic acid). Journal of Applied Polymer Science 108(2) (2008): 870-875.

[8] Nofar, M., Tabatabaei, A., and Park, C.B. Effects of nano-/micro-sized additives on the crystallization behaviors of PLA and PLA/CO2 mixtures. Polymer 54(9) (2013): 2382-2391.

[9] Díez-Gutiérrez, S., Rodríguez-Pérez, M.A., De Saja, J.A., and Velasco, J.I. Dynamic mechanical analysis of injection-moulded discs of polypropylene and untreated and silane-treated talc-filled polypropylene composites. Polymer 40(19) (1999): 5345-5353.

[10] Leong, Y.W., Bakar, M.B.A., Mohd. Ishak, Z.A., and Ariffin, A. Effects of filler treatments on the mechanical, flow, thermal, and morphological properties of talc and calcium carbonate filled polypropylene hybrid composites. Journal of Applied Polymer Science 98(1) (2005): 413-426.

[11] Yu, F., Liu, T., Zhao, X., Yu, X., Lu, A., and Wang, J. Effects of talc on the mechanical and thermal properties of polylactide. Journal of Applied Polymer Science 125(S2) (2012): E99-E109.

[12] Pracella, M. Crystallization of Polymer Blends. in Handbook of Polymer Crystallization, pp. 287-326: John Wiley & Sons, Inc., 2013.

[13] Xiao, H.W., Li, P., Ren, X., Jiang, T., and Yeh, J.-T. Isothermal crystallization kinetics and crystal structure of poly(lactic acid): Effect of triphenyl phosphate and talc. Journal of Applied Polymer Science 118(6) (2010): 3558-3569.

[14] Piorkowska, E. and Rutledge, G.C. Handbook of polymer crystallization. John Wiley & Sons, 2013.

[15] Kaavessina, M., Ali, I., Elleithy, R.H., and Al-Zahrani, S.M. Crystallization behavior of poly(lactic acid)/elastomer blends. Journal of Polymer Research 19(2) (2012): 1-12.

[16] Tri, P.N., Domenek, S., Guinault, A., and Sollogoub, C. Crystallization behavior of poly(lactide)/poly(β-hydroxybutyrate)/talc composites. Journal of Applied Polymer Science 129(6) (2013): 3355-3365.

[17] Henricks, J., Boyum, M., and Zheng, W. Crystallization kinetics and structure evolution of a polylactic acid during melt and cold crystallization. Journal of Thermal Analysis and Calorimetry 120(3) (2015): 1765-1774.

[18] Liu, T., et al. Isothermal Crystallization Kinetics of Fiber/Polylactic Acid Composites and Morphology. Polymer-Plastics Technology and Engineering 51(6) (2012): 597-604.

[19] Mei, Z. and Chung, D. Cold-crystallisation of polyphenylene sulphide, studied by measuring the electrical resistance of a carbon-fibre polyphenylene-sulphide-matrix composite. Polymer and Polymer Composites 8(5) (2000): 319-324.

[20] Wellen, R.M.R. and Rabello, M.S. The kinetics of isothermal cold crystallization and tensile properties of poly(ethylene terephthalate). Journal of Materials Science 40(23) (2005): 6099-6104.

[21] Wellen, R.M.R. and Rabello, M.S. Non-isothermal cold crystallization kinetics and morphology of PET + SAN blends. Journal of Applied Polymer Science 116(2) (2010): 1077-1087.

[22] Ziaee, Z. and Supaphol, P. Non-isothermal melt- and cold-crystallization kinetics of poly(3-hydroxybutyrate). Polymer Testing 25(6) (2006): 807-818.

[23] Kiflie, Z., Piccarolo, S., Brucato, V., and Baltá-Calleja, F.J. Role of thermal history on quiescent cold crystallization of PET. Polymer 43(16) (2002): 4487-4493.

[24] Yu, L., Liu, H., Dean, K., and Chen, L. Cold crystallization and postmelting crystallization of PLA plasticized by compressed carbon dioxide. Journal of Polymer Science Part B: Polymer Physics 46(23) (2008): 2630-2636.

[25] Lorenzo, A.T., Arnal, M.L., Albuerne, J., and Müller, A.J. DSC isothermal polymer crystallization kinetics measurements and the use of the Avrami equation to fit the data: guidelines to avoid common problems. Polymer Testing 26(2) (2007): 222-231.

[26] Wei, Z., et al. Insight into the annealing peak and microstructural changes of poly(l-lactic acid) by annealing at elevated temperatures. Polymer 54(13) (2013): 3377-3384.

[27] Kong, Y. and Hay, J.N. The effect of annealing on the crystallization of poly(ethylene terephthalate)/polycarbonate blends. Journal of Polymer Science Part B: Polymer Physics 42(11) (2004): 2129-2136.

[28] Huang, J.M., Chu, P.P., and Chang, F.C. Conformational changes and molecular motion of poly(ethylene terephthalate) annealed above glass transition temperature. Polymer 41(5) (2000): 1741-1748.

[29] Tabi, T., Sajó, I., Szabó, F., Luyt, A., and Kovács, J. Crystalline structure of annealed polylactic acid and its relation to processing. Express Polym Lett 4(10) (2010): 659-668.

[30] Nagarajan, V., Zhang, K., Misra, M., and Mohanty, A.K. Overcoming the Fundamental Challenges in Improving the Impact Strength and Crystallinity of

PLA Biocomposites: Influence of Nucleating Agent and Mold Temperature. ACS Applied Materials & Interfaces 7(21) (2015): 11203-11214.

[31] Ke, T. and Sun, X. Melting behavior and crystallization kinetics of starch and poly(lactic acid) composites. Journal of Applied Polymer Science 89(5) (2003): 1203-1210.

[32] van Soest, J.J.G. and Vliegenthart, J.F.G. Crystallinity in starch plastics: consequences for material properties. Trends in Biotechnology 15(6) (1997): 208-213.

[33] Tjong, S.C. and Xu, S.A. Non-isothermal crystallization kinetics of calcium carbonate-filled β-crystalline phase polypropylene composites. Polymer International 44(1) (1997): 95-103.

[34] Velasco, J.I., De Saja, J.A., and Martínez, A.B. FRACTURE BEHAVIOUR OF UNTREATED AND SILANE-TREATED TALC-FILLED POLYPROPYLENE COMPOSITES. Fatigue & Fracture of Engineering Materials & Structures 20(5) (1997): 659-670.

[35] Choi, J., Kim, S.G., and Laine, R.M. Organic/inorganic hybrid epoxy nanocomposites from aminophenylsilsesquioxanes. Macromolecules 37(1) (2004): 99-109.

[36] Velasco, J.I., De Saja, J.A., and Martínez, A.B. Crystallization behavior of polypropylene filled with surface-modified talc. Journal of Applied Polymer Science 61(1) (1996): 125-132.

[37] Abdelmouleh, M., Boufi, S., Belgacem, M.N., and Dufresne, A. Short natural-fibre reinforced polyethylene and natural rubber composites: Effect of silane coupling agents and fibres loading. Composites Science and Technology 67(7–8) (2007): 1627-1639.

[38] Chen, J., Li, X., and Wu, C. Crystallization Behavior of Polypropylene Filled with Modified Carbon Black. Polym. J 39(7) (2007): 722-730.

APPENDICES

APPENDIX A

CALCULATION FOR THE PLA COMPOSITES

The calculation of PLA composites is shown as an example as explain below. However, other composites can also be calculated in the similar conditions.

Important information

Density of PLA	1.24	g/cm^3
Density of talc	0.61	g/cm^3
Density of $CaCO_3$	1.25	g/cm^3
Density of cassava starch	0.65	g/cm^3

Condition 1 Calculation of the PLA/Talc (95/5 vol%)

$$\text{Volume of talc} = \frac{\left[\frac{\text{Weight of talc}}{\text{Density of talc}}\right]}{\left[\frac{\text{Weight of Poly(lactic acid)}}{\text{Density of Poly(lactic acid)}}\right]+\left[\frac{\text{Total PLA/Talc - Weight of Poly(lactic acid)}}{\text{Density of talc}}\right]}$$

$$0.05 = \frac{\left[\frac{\text{Weight of talc}}{0.611}\right]}{\left[\frac{\text{Weight of Poly(lactic acid)}}{1.24}\right]+\left[\frac{\text{1,500 g - Weight of Poly(lactic acid)}}{0.611}\right]}$$

∴ Total Poly(lactic acid) used in this experiment was 1,500 g

Total talc used in this experiment was 39.4 g

Condition 2 Calculation of the PLA/$CaCO_3$ (95/5 vol%)

$$\text{Volume of } CaCO_3 = \frac{\left[\frac{\text{Weight of } CaCO_3}{\text{Density of } CaCO_3}\right]}{\left[\frac{\text{Weight of Poly(lactic acid)}}{\text{Density of Poly(lactic acid)}}\right]+\left[\frac{\text{Total PLA/}CaCO_3\text{ - Weight of Poly(lactic acid)}}{\text{Density of } CaCO_3}\right]}$$

$$0.05 = \frac{\left[\frac{\text{Weight of } CaCO_3}{1.250}\right]}{\left[\frac{\text{Weight of Poly(lactic acid)}}{1.24}\right]+\left[\frac{\text{1,500 g - Weight of Poly(lactic acid)}}{1.250}\right]}$$

∴ Total Poly(lactic acid) used in this experiment was 1,500 g

Total $CaCO_3$ used in this experiment was 80.6 g

Condition 3 Calculation of the PLA/Starch (95/5 vol%)

$$\text{Volume of starch} = \frac{\left[\frac{\text{Weight of starch}}{\text{Density of starch}}\right]}{\left[\frac{\text{Weight of Poly(lactic acid)}}{\text{Density of Poly(lactic acid)}}\right]+\left[\frac{\text{Total PLA/Talc - Weight of Poly(lactic acid)}}{\text{Density of starch}}\right]}$$

$$0.05 = \frac{\left[\frac{\text{Weight of talc}}{0.650}\right]}{\left[\frac{\text{Weight of Poly(lactic acid)}}{1.24}\right]+\left[\frac{\text{1,500 g - Weight of Poly(lactic acid)}}{0.650}\right]}$$

∴ Total Poly(lactic acid) used in this experiment was 1,500 g

Total starch used in this experiment was 41.9 g

APPENDIX B

THERMAL PROPERTIES

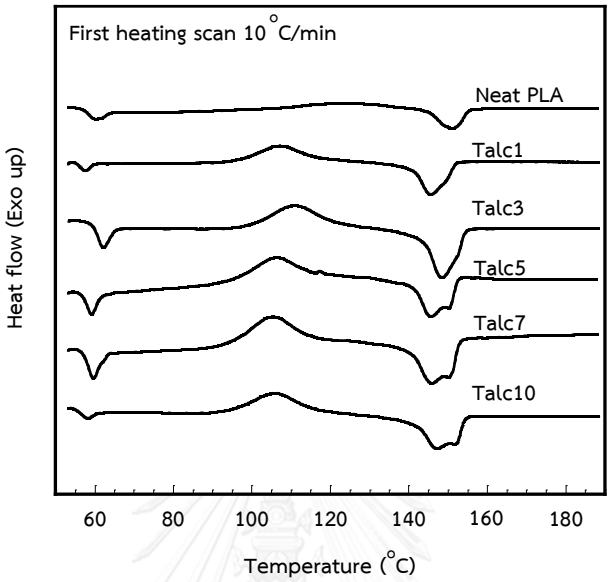

Figure B.1 DSC thermograms in the first heating scan of PLA/Talc

Table B.1 Thermal properties of PLA/Talc in the first heating scan

Sample	$T_{g\ PLA}$ (°C)	T_{cc} (°C)	T_{m1} (°C)	T_{m2} (°C)	ΔH_{cc} (J/g)	ΔH_m (J/g)	$\%X_c$
Neat PLA	58.0	126.0	149.7		4.6	10.1	6.1
Talc1	58.8	107.2	148.7		20.7	27.7	7.6
Talc3	58.7	110.7	148.7		19.1	27.2	8.9
Talc5	58.6	105.9	145.8	150.6	18.5	29.0	11.5
Talc7	58.8	105.5	146.1	150.5	18.0	27.9	11.1
Talc10	58.8	106.0	147.2	151.0	16.8	29.1	14.0

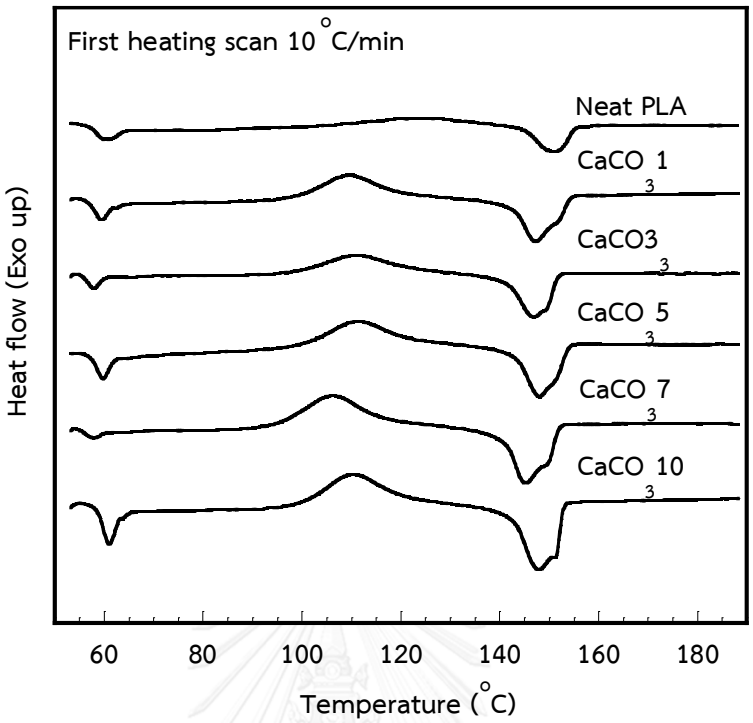

Figure B.2 DSC thermograms in the first heating scan of PLA/$CaCO_3$

Table B.2 Thermal properties of PLA/$CaCO_3$ in the first heating scan

Sample	$T_{g\ PLA}$ (°C)	T_{cc} (°C)	T_{m1} (°C)	T_{m2} (°C)	ΔH_{cc} (J/g)	ΔH_m (J/g)	$\%X_c$
Neat PLA	58.2	126.0	149.7		4.6	10.1	6.1
$CaCO_3$1	58.8	109.3	147.2	152.1	21.2	26.3	5.5
$CaCO_3$3	58.8	110.8	146.9	149.7	18.9	26.3	8.3
$CaCO_3$5	58.7	111.3	148.2	151.9	18.3	26.4	9.3
$CaCO_3$7	58.8	106.5	145.5	149.9	19.3	27.9	10.2
$CaCO_3$10	58.9	110.3	147.9	151.6	17.3	27.5	12.5

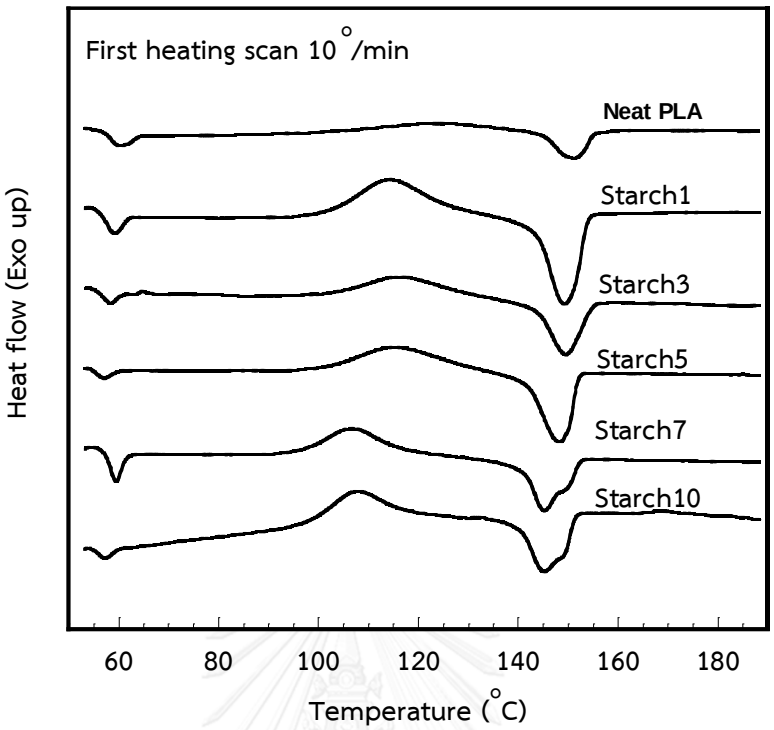

Figure B.3 DSC thermograms in the first heating scan of PLA/Starch

Table B.3 Thermal properties of PLA/Starch in the first heating scan

Sample	$T_{g\ PLA}$ (°C)	T_{cc} (°C)	T_{m1} (°C)	T_{m2} (°C)	ΔH_{cc} (J/g)	ΔH_m (J/g)	$\%X_c$
Neat PLA	58.2	126.0	149.7		4.6	10.1	6.1
Starch1	58.7	105.4	149.2		20.3	20.3	5.6
Starch3	58.7	116.1	149.7		19.2	19.2	5.8
Starch5	58.6	115.6	148.2	151.7	19.7	19.7	6.0
Starch7	58.7	106.9	145.3	150.2	20.5	20.5	7.2
Starch10	58.6	107.6	145.3	149.3	17.9	17.9	8.3

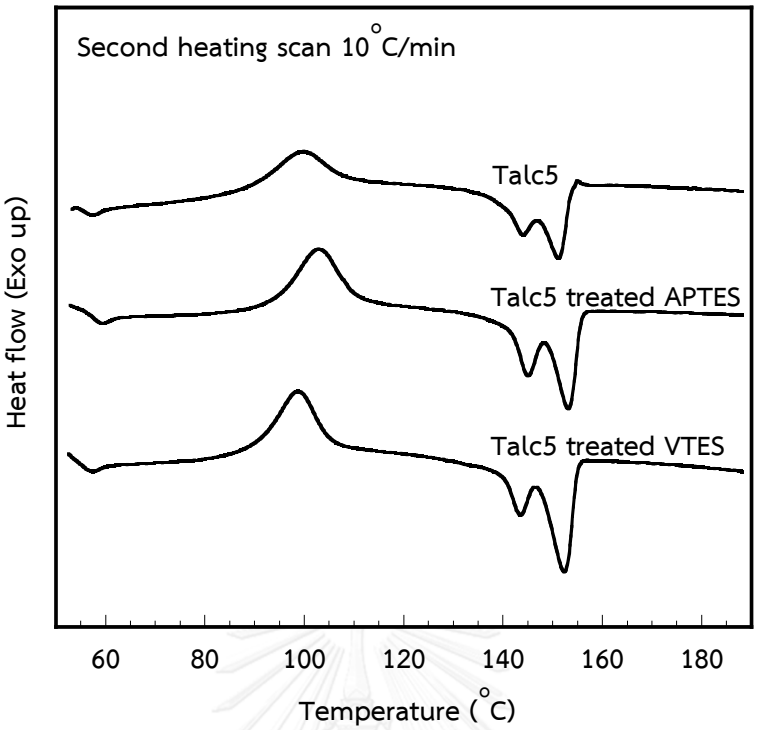

Figure B.4 DSC thermograms in the first heating scan of untreated Talc5, APTES-Talc5 and VTES-Talc5

Table B.4 Thermal properties of untreated Talc5, APTES-Talc5 and VTES-Talc5 in the first heating scan

Sample	$T_{g\ PLA}$ (°C)	T_{cc} (°C)	T_{m1} (°C)	T_{m2} (°C)	ΔH_{cc} (J/g)	ΔH_m (J/g)	$\%X_c$
Untreated Talc5	58.6	100.5	143.8	151.1	19.9	29.2	10.3
APTES-Talc5	58.8	106.9	146.2	152.2	20.1	30.4	11.4
VTES-Talc5	58.4	106.4	145.5	151.7	19.0	27.3	9.1

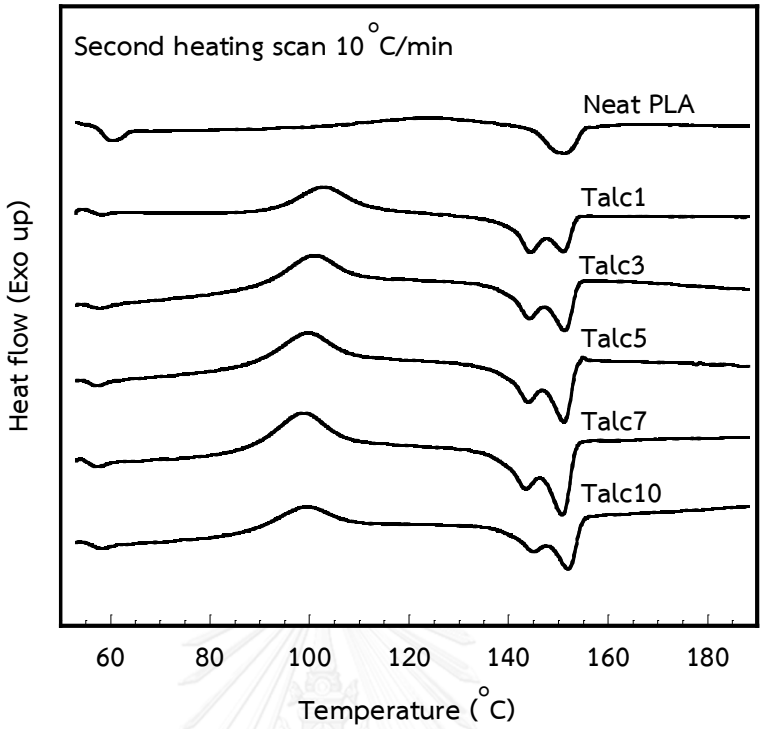

Figure B.5 DSC thermograms in the second heating scan of PLA/Talc

Table B.5 Thermal properties of PLA/Talc in the second heating scan

Sample	$T_{g\ PLA}$ (°C)	T_{cc} (°C)	T_{m1} (°C)	T_{m2} (°C)	ΔH_{cc} (J/g)	ΔH_m (J/g)	$\%X_c$
Neat PLA	58.8	126.0	149.7		4.6	10.1	6.1
Talc1	58.8	102.8	144.4	151.2	22.6	30.4	8.7
Talc3	58.6	110.3	147.7	151.2	18.4	26.6	9.1
Talc5	58.6	99.9	143.8	151.1	19.9	29.2	10.3
Talc7	58.8	98.5	143.4	150.9	17.8	30.7	14.3
Talc10	58.8	99.5	144.9	152.0	15.5	29.4	15.4

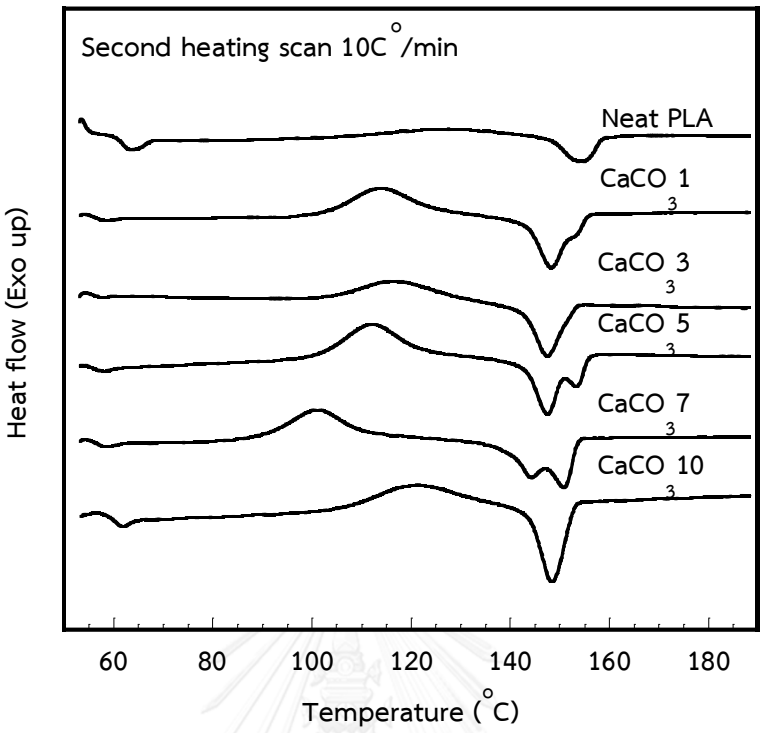

Figure B.6 DSC thermograms in the second heating scan of PLA/$CaCO_3$

Table B.6 Thermal properties of PLA/$CaCO_3$ in the second heating scan

Sample	$T_{g\ PLA}$ (°C)	T_{cc} (°C)	T_{m1} (°C)	T_{m2} (°C)	ΔH_{cc} (J/g)	ΔH_m (J/g)	$\%X_c$
Neat PLA	58.8	126.0	149.7		4.6	10.1	6.1
$CaCO_3$1	58.8	114.2	148.2	153.7	23.2	29.5	6.9
$CaCO_3$3	58.9	116.7	147.6	150.7	20.5	28.0	8.3
$CaCO_3$5	58.7	112.0	147.5	153.7	22.1	30.1	8.8
$CaCO_3$7	58.9	101.2	143.9	150.9	20.0	28.4	9.3
$CaCO_3$10	58.9	120.5	148.6	152.1	15.1	22.7	8.4

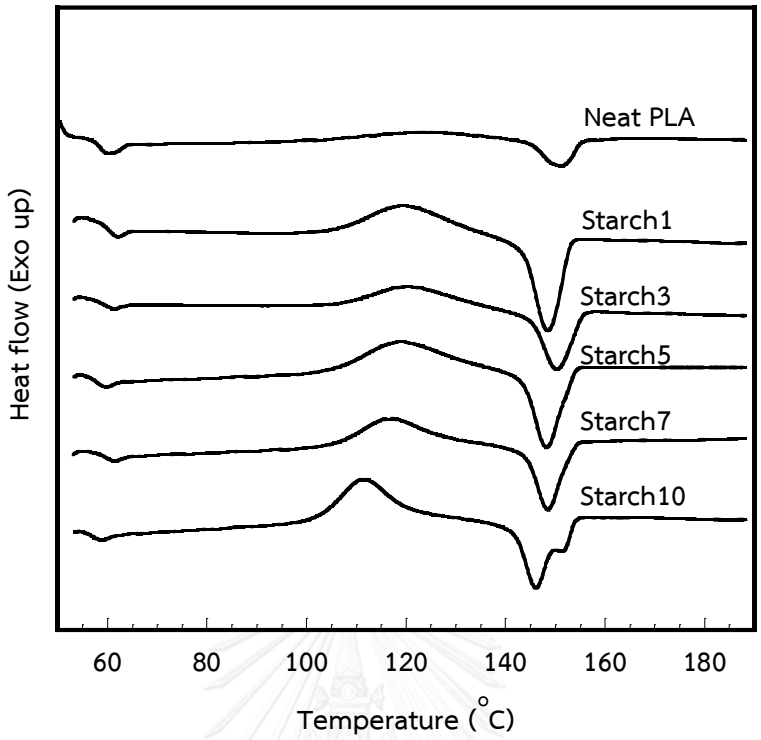

Figure B.7 DSC thermograms in the second heating scan of PLA/Starch

Table B.7 Thermal properties of PLA/Starch in the second heating scan

Sample	$T_{g\ PLA}$ (°C)	T_{cc} (°C)	T_{m1} (°C)	T_{m2} (°C)	ΔH_{cc} (J/g)	ΔH_m (J/g)	$\%X_c$
Neat PLA	58.8	126.0	149.7		4.6	10.1	6.1
Starch1	58.8	119.9	148.5		16.9	22.3	6.0
Starch3	58.8	120.4	150.4		19.7	25.1	6.0
Starch5	58.7	118.2	148.3	151.2	21.7	27.2	6.0
Starch7	58.7	117.3	148.7	151.5	21.0	28.0	7.7
Starch10	58.7	111.7	146.2	152.0	21.0	28.5	8.4

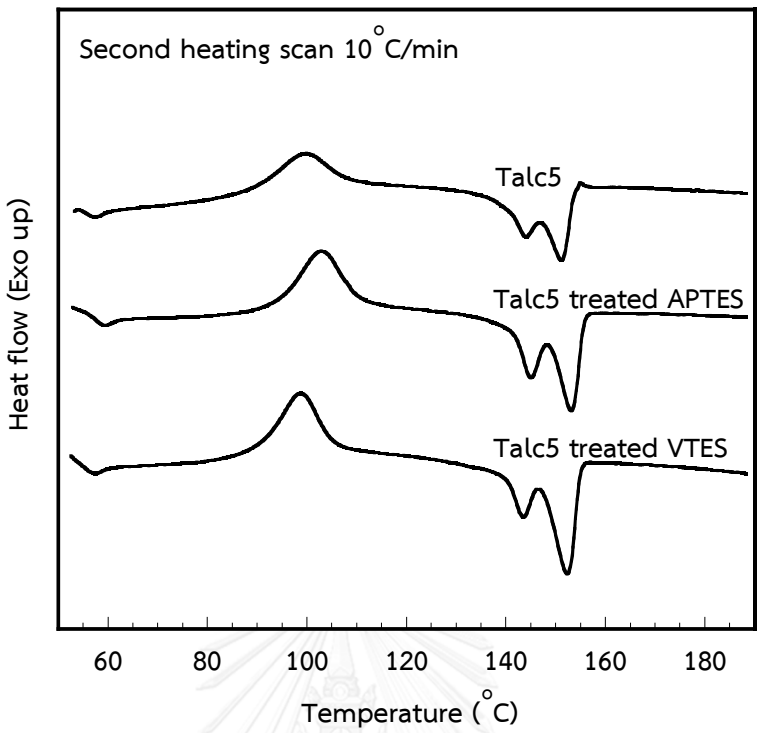

Figure B.8 DSC thermograms of untreated Talc5, APTES-Talc5 and VTES-Talc5 from the second heating scan

Table B.8 Thermal properties of untreated Talc5, APTES-Talc5 and VTES-Talc5 from the second heating scan

Sample	$T_{g\ PLA}$ (°C)	T_{cc} (°C)	T_{m1} (°C)	T_{m2} (°C)	ΔH_{cc} (J/g)	ΔH_m (J/g)	$\%X_c$
Untreated Talc5	58.6	99.9	144.1	151.3	22.6	30.4	10.3
APTES-Talc5	58.4	102.8	145.0	153.2	22.6	33.7	12.3
VTES-Talc5	58.6	98.8	143.4	152.3	21.4	33.1	12.9

APPENDIX C

ISOTHERMAL COLD-CRYSTALLIZATION KINETICS

Table C.1 Isothermal crystallization kinetic parameters calculated from Avrami model for neat PLA and its composites at different crystallization temperatures and filler contents.

Sample	T_c (°C)	Avrami index (n)	K (min^{-1})	$t_{1/2, exp}$ (min)	$t_{1/2, cal}$ (min)	R^2
Neat PLA	90	2.6	$1.55x10^{-3}$	9.1	10.7	0.9990
	100	2.9	$5.43x10^{-3}$	4.6	5.2	0.9995
	110	3.7	$9.30x10^{-4}$	5.2	6.0	0.9998
	120	3.9	$8.85x10^{-5}$	8.8	9.4	0.9999
	130	4.0	$1.22x10^{-5}$	16.9	24.5	0.9999
PLA/Talc 1 vol%	90	2.9	$5.87x10^{-3}$	4.7	5.0	0.9997
	100	3.2	$2.52x10^{-2}$	2.8	2.8	0.9997
	110	3.5	$1.36x10^{-2}$	2.7	3.0	0.9998
	120	2.6	$1.48x10^{-2}$	4.0	4.2	0.9997
	130	2.4	$3.54x10^{-3}$	7.1	9.3	0.9994
PLA/Talc 3 vol%	90	2.8	$1.03x10^{-2}$	3.5	3.9	0.9995
	100	2.4	$6.86x10^{-2}$	2.3	2.5	0.9993
	110	3.2	$2.53x10^{-2}$	2.5	2.8	0.9995
	120	2.3	$3.74x10^{-2}$	3.2	3.5	0.9999
	130	2.3	$7.01x10^{-2}$	7.2	7.6	1.0000
PLA/Talc 5 vol%	90	2.8	$3.40x10^{-2}$	3.3	3.3	0.9983
	100	3.4	$3.74x10^{-2}$	2.0	2.3	1.0000
	110	3.3	$2.35x10^{-2}$	2.0	2.8	0.9990
	120	2.9	$2.71x10^{-2}$	3.2	3.5	0.9998
	130	2.3	$8.56x10^{-3}$	6.2	6.7	0.9999

Sample	T_c (°C)	Avrami index (n)	K (min^{-1})	$t_{1/2}$ exp (min)	$t_{1/2}$ cal (min)	R^2
PLA/Talc	90	2.3	$3.24x10^{-2}$	3.6	3.7	0.9996
7 vol%	100	2.7	$6.78x10^{-2}$	2.0	2.3	0.9998
	110	2.5	$6.01x10^{-2}$	2.2	2.6	0.9994
	120	2.2	$4.73x10^{-2}$	3.1	3.4	0.9998
	130	2.0	$1.21x10^{-2}$	7.0	7.3	0.9999
PLA/Talc	90	2.4	$1.77x10^{-2}$	3.8	4.5	0.9999
10 vol%	100	2.5	$8.16x10^{-2}$	2.0	2.3	0.9999
	110	2.8	$9.99x10^{-2}$	1.8	2.2	0.9997
	120	2.2	$4.83x10^{-2}$	2.9	3.4	0.9998
	130	2.0	$1.83x10^{-2}$	6.0	6.6	1.0000
PLA/$CaCO_3$	90	3.4	$2.18x10^{-3}$	4.9	5.4	0.9998
1 vol%	100	3.7	$9.59x10^{-3}$	2.6	3.1	0.9996
	110	3.7	$9.01x10^{-3}$	2.6	3.2	0.9998
	120	3.2	$3.91x10^{-3}$	4.6	4.9	0.9999
	130	2.6	$1.11x10^{-3}$	11.1	11.9	0.9998
PLA/$CaCO_3$	90	3.2	$3.04x10^{-3}$	4.8	5.3	0.9999
3 vol%	100	3.5	$1.14x10^{-2}$	2.6	3.2	0.9998
	110	3.7	$3.95x10^{-3}$	3.3	3.7	0.9998
	120	3.6	$1.08x10^{-3}$	4.8	6.0	0.9997
	130	2.3	$1.89x10^{-3}$	11.9	13.0	0.9999
PLA/$CaCO_3$	90	3.2	$2.70x10^{-3}$	5.3	5.5	0.9998
5 vol%	100	3.6	$8.71x10^{-3}$	3.2	3.3	0.9998
	110	3.7	$3.95x10^{-3}$	3.4	4.0	0.9998
	120	3.8	$6.56x10^{-4}$	5.3	6.2	0.9998
	130	3.1	$2.12x10^{-4}$	12.1	13.2	0.9997

Sample	T_c (°C)	Avrami index (n)	K (min^{-1})	$t_{1/2}$ exp (min)	$t_{1/2}$ cal (min)	R^2
PLA/$CaCO_3$	90	3.3	$2.52x10^{-3}$	5.0	5.5	0.9997
7 vol%	100	3.8	$5.18x10^{-3}$	3.1	3.5	0.9997
	110	3.4	$7.08x10^{-3}$	3.4	3.8	0.9994
	120	3.5	$1.71x10^{-3}$	5.0	5.6	0.9997
	130	2.2	$3.80x10^{-3}$	10.1	11.1	0.9874
PLA/$CaCO_3$	90	3.7	$9.80x10^{-4}$	5.0	5.9	0.9998
10 vol%	100	3.8	$3.83x10^{-3}$	3.0	3.8	0.9997
	110	3.4	$6.65x10^{-3}$	3.7	3.9	0.9990
	120	3.6	$8.62x10^{-4}$	5.6	6.4	0.9995
	130	2.5	$8.39x10^{-4}$	12.3	14.4	0.9960
PLA/Starch	90	3.3	$1.80x10^{-3}$	6.0	6.1	0.9999
1 vol%	100	3.8	$4.89x10^{-3}$	3.2	3.6	0.9995
	110	4.0	$1.41x10^{-3}$	4.0	4.5	0.9997
	120	3.9	$5.70x10^{-4}$	5.6	6.2	0.9995
	130	2.6	$6.60x10^{-4}$	12.6	14.5	0.9995
PLA/Starch	90	3.4	$9.74x10^{-4}$	6.0	6.7	0.9999
3 vol%	100	3.4	$6.69x10^{-3}$	3.4	3.6	0.9998
	110	4.1	$1.88x10^{-4}$	3.4	4.3	0.9998
	120	3.8	$6.25x10^{-4}$	5.5	6.3	0.9997
	130	3.1	$1.36x10^{-4}$	12.3	16.5	0.9995
PLA/Starch	90	3.4	$8.90x10^{-4}$	6.5	7.1	0.9999
5 vol%	100	3.5	$4.50x10^{-3}$	3.7	4.2	0.9997
	110	3.9	$1.76x10^{-3}$	3.6	4.4	0.9998
	120	4.5	$9.13x10^{-5}$	6.3	7.2	0.9996
	130	3.8	$9.29x10^{-6}$	16.2	15.7	0.9997

Sample	T_c (°C)	Avrami index (n)	K (min^{-1})	$t_{1/2}$ exp (min)	$t_{1/2}$ cal (min)	R^2
PLA/Starch 7 vol%	90	3.7	$1.79x10^{-3}$	5.1	5.1	0.9997
	100	4.2	$2.72x10^{-3}$	3.4	3.7	0.9994
	110	3.5	$4.64x10^{-3}$	3.4	4.1	0.9997
	120	4.1	$1.80x10^{-4}$	6.0	7.3	0.9990
	130	4.7	$7.37x10^{-7}$	9.8	18.2	0.9965
PLA/Starch 10 vol%	90	3.9	$3.21x10^{-4}$	6.4	7.2	0.9999
	100	3.9	$8.78x10^{-4}$	4.3	5.3	0.9997
	110	3.7	$3.87x10^{-4}$	6.7	7.4	0.9997
	120	3.9	$6.29x10^{-5}$	9.7	10.3	0.9998
	130	4.5	$1.85x10^{-7}$	15.9	22.0	0.9998

Table C.2 Isothermal crystallization kinetic parameters calculated from Avrami model for untreated Talc5, APTES-Talc5 and VTES-Talc5 films at crystallization temperature of 100°C.

Sample	T_c (°C)	Avrami index (n)	K (min^{-1})	$t_{1/2}$ exp (min)	$t_{1/2}$ cal (min)	R^2
APTES-Talc5	100	3.2	$5.93x10^{-2}$	1.9	1.9	0.9997
VTES-Talc5	100	3.6	$7.82x10^{-2}$	1.9	1.9	1.000

APPENDIX D

MECHANICAL PROPERTIES

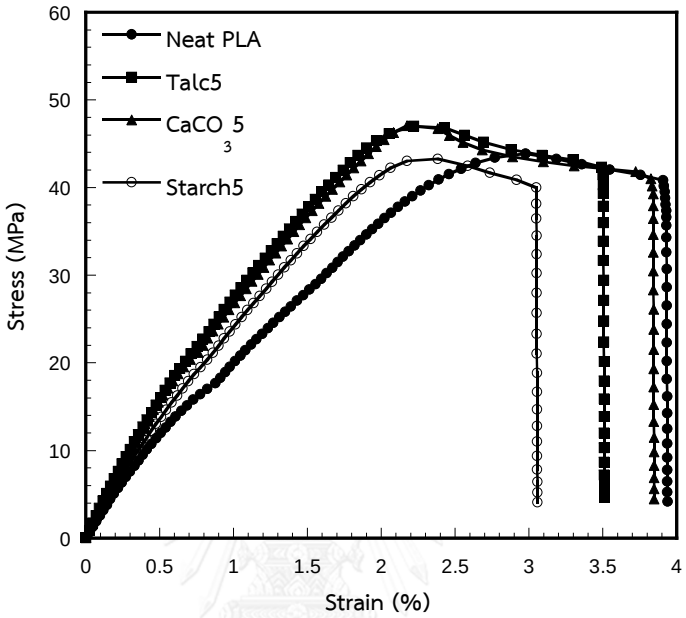

Figure D.1 Stress strain curve of PLA and PLA composites of PLA cast films

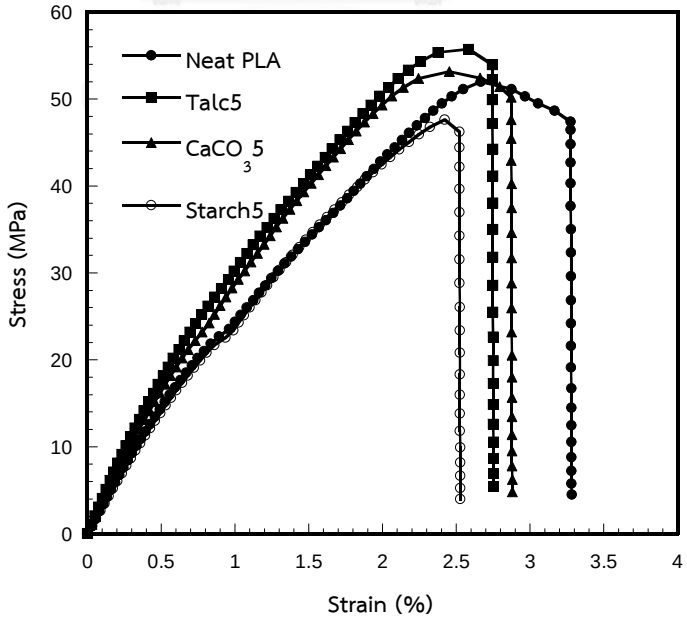

Figure D.2 Stress strain curve of PLA and PLA composites of PLA thermoforming films

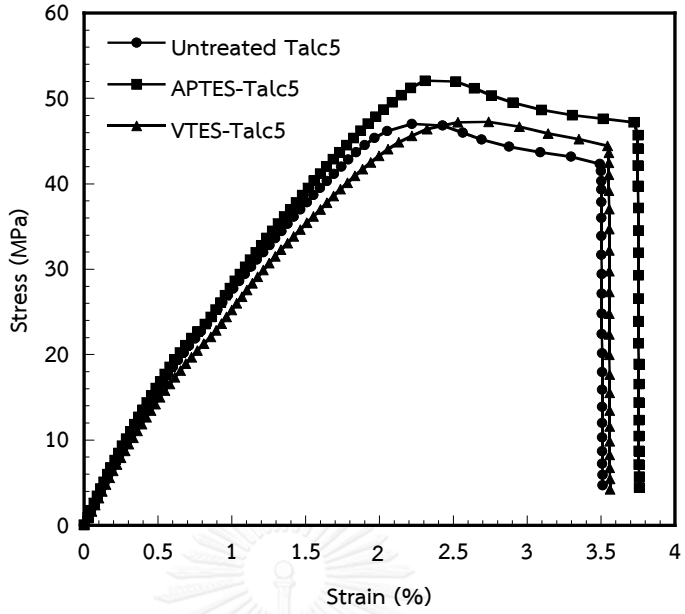

Figure D.3 Stress strain curve of untreated and treated talc5 of PLA cast films

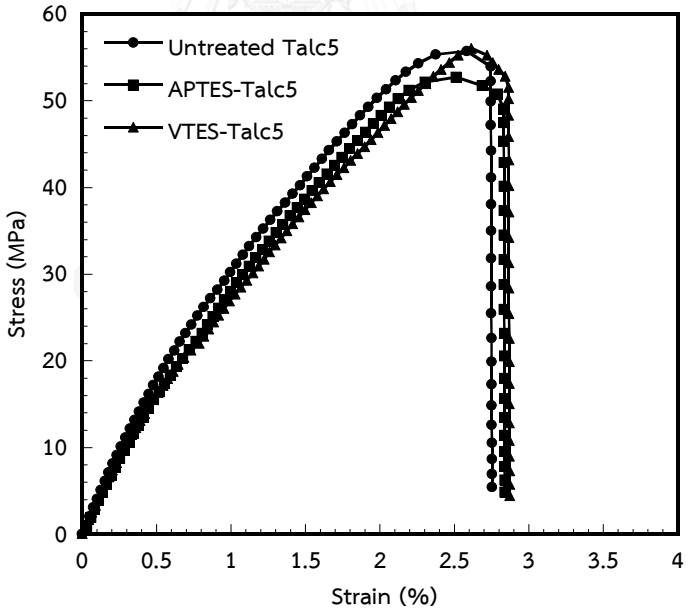

Figure D.4 Stress strain curve of untreated and treated talc5 of PLA thermoforming films

Table D.1 Tensile properties in sheet films of Neat PLA

Sample no.	Tensile strength (MPa)	Young's Modulus (MPa)	Elongation at break (%)	Tensile toughness (mJ)
1	47.7	1813.3	3.7	454.0
2	44.8	1729.6	3.8	402.7
3	44.8	1793.7	3.6	436.6
4	43.9	1807.1	3.4	420.1
5	40.1	1841.5	3.6	477.8
Avg.	44.3	1797.0	3.6	438.2
S.D.	2.7	41.6	0.1	29.2

Table D.2 Tensile properties in thermoforming process of Neat PLA

Sample no.	Tensile strength (MPa)	Young's Modulus (MPa)	Elongation at break (%)	Tensile toughness (mJ)
1	47.7	1813.3	3.7	454.0
2	44.8	1729.6	3.8	402.7
3	44.8	1793.7	3.6	436.6
4	43.9	1807.1	3.4	420.1
5	40.1	1841.5	3.6	477.8
Avg.	44.3	1797.0	3.6	438.2
S.D.	2.7	41.6	0.1	29.2

Table D.3 Tensile properties in sheet films of PLA/Talc 1 vol%

Sample no.	Tensile strength (MPa)	Young's Modulus (MPa)	Elongation at break (%)	Tensile toughness (mJ)
1	47.3	2115.2	3.6	439.3
2	47.6	2121.1	5.0	464.5
3	50.0	2187.4	3.6	623.5
4	47.7	2170.3	5.0	515.2
5	48.4	2162.2	3.8	312.2
Avg.	48.2	2151.3	4.2	470.9
S.D.	1.1	31.6	0.8	113.5

Table D.4 Tensile properties in thermoforming process of PLA/Talc 1 vol%

Sample no.	Tensile strength (MPa)	Young's Modulus (MPa)	Elongation at break (%)	Tensile toughness (mJ)
1	53.9	2121.3	3.3	383.6
2	54.1	2079.8	3.4	397.8
3	54.4	2095.0	3.3	383.6
4	54.5	2117.9	3.5	391.5
5	53.9	2091.7	3.2	391.2
Avg.	54.2	2101.1	3.4	389.5
S.D.	0.3	17.8	0.1	6.0

Table D.5 Tensile properties in sheet films of PLA/Talc 5 vol%

Sample no.	Tensile strength (MPa)	Young's Modulus (MPa)	Elongation at break (%)	Tensile toughness (mJ)
1	48.0	2256.4	3.2	373.3
2	49.2	2117.0	3.5	359.9
3	47.4	2155.8	3.6	324.3
4	47.0	2293.9	3.5	324.5
5	49.1	2166.0	3.0	359.0
Avg.	48.2	2197.8	3.4	348.2
S.D.	1.0	74.1	0.2	22.5

Table D.6 Tensile properties in thermoforming process of PLA/Talc 5 vol%

Sample no.	Tensile strength (MPa)	Young's Modulus (MPa)	Elongation at break (%)	Tensile toughness (mJ)
1	55.9	2362.8	2.8	312.3
2	56.5	2426.2	2.6	319.9
3	55.8	2424.6	2.7	291.2
4	55.4	2429.8	2.8	271.3
5	54.5	2341.5	2.7	330.2
Avg.	55.6	2397.0	2.7	305.0
S.D.	0.8	41.7	0.1	23.6

Table D.7 Tensile properties in sheet films of PLA/Talc 10 vol%

Sample no.	Tensile strength (MPa)	Young's Modulus (MPa)	Elongation at break (%)	Tensile toughness (mJ)
1	47.5	2146.6	3.0	311.3
2	48.2	2165.7	3.0	307.3
3	47.0	2178.6	3.2	313.5
4	50.4	2157.8	3.4	312.3
5	49.5	2215.6	3.1	313.0
Avg.	48.5	2172.9	3.1	311.5
S.D.	1.4	26.6	0.2	2.5

Table D.8 Tensile properties in thermoforming process of PLA/Talc 10 vol%

Sample no.	Tensile strength (MPa)	Young's Modulus (MPa)	Elongation at break (%)	Tensile toughness (mJ)
1	55.5	2319.4	2.7	253.1
2	54.5	2268.2	2.6	254.7
3	53.2	2249.9	2.6	250.6
4	56.8	2366.4	2.7	245.4
5	54.7	2496.5	2.6	262.1
Avg.	54.9	2340.1	2.6	253.2
S.D.	1.3	98.6	0.1	6.1

Table D.9 Tensile properties in sheet films of PLA/$CaCO_3$ 5 vol%

Sample no.	Tensile strength (MPa)	Young's Modulus (MPa)	Elongation at break (%)	Tensile toughness (mJ)
1	47.7	2047.0	3.3	408.8
2	47.1	1963.8	3.4	390.7
3	47.8	2164.0	3.1	394.4
4	47.0	2147.2	3.4	424.9
5	47.3	1912.2	3.6	394.4
Avg.	47.4	2046.8	3.4	402.6
S.D.	0.4	110.5	0.2	14.3

Table D.10 Tensile properties in thermoforming process of PLA/$CaCO_3$ 5 vol%

Sample no.	Tensile strength (MPa)	Young's Modulus (MPa)	Elongation at break (%)	Tensile toughness (mJ)
1	53.4	2351.6	2.8	347.1
2	53.0	2387.7	2.9	336.8
3	54.2	2375.7	2.9	270.7
4	53.1	2401.1	2.8	333.2
5	53.2	2324.9	2.9	284.9
Avg.	53.4	2368.2	2.9	314.6
S.D.	0.5	30.3	0.0	34.3

Table D.11 Tensile properties in sheet films of PLA/Starch 5 vol%

Sample no.	Tensile strength (MPa)	Young's Modulus (MPa)	Elongation at break (%)	Tensile toughness (mJ)
1	41.0	1966.1	2.6	240.9
2	42.2	1923.7	2.3	241.9
3	42.2	1983.7	2.3	242.0
4	41.6	1925.2	2.6	245.0
5	42.0	1906.3	2.6	260.8
Avg.	41.8	1941.0	2.5	246.1
S.D.	0.5	32.4	0.2	8.4

*T*able D.12 Tensile properties in thermoforming process of PLA/Starch 5 vol%

Sample no.	Tensile strength (MPa)	Young's Modulus (MPa)	Elongation at break (%)	Tensile toughness (mJ)
1	47.8	2052.5	2.3	207.5
2	48.3	2151.5	2.3	229.5
3	47.7	2015.6	2.3	205.6
4	47.5	2006.7	2.4	207.5
5	47.9	2110.5	2.2	206.1
Avg.	47.8	2067.4	2.3	211.2
S.D.	0.3	62.3	0.1	10.3

Table D.13 Tensile properties in sheet films of PLA/Talc 5 vol% treated with 3-aminopropyltriethoyxsilane (APTES)

Sample no.	Tensile strength (MPa)	Young's Modulus (MPa)	Elongation at break (%)	Tensile toughness (mJ)
1	50.4	2405.3	3.3	343.0
2	52.1	2366.9	3.3	349.7
3	50.5	2344.5	3.1	332.1
4	50.0	2346.5	3.1	387.2
5	50.0	2420.4	3.2	355.7
Avg.	50.6	2376.7	3.2	353.5
S.D.	0.9	34.6	0.1	20.7

Table D.14 Tensile properties in thermoforming process of PLA/Talc 5 vol% treated with 3-aminopropyltriethoyxsilane (APTES)

Sample no.	Tensile strength (MPa)	Young's Modulus (MPa)	Elongation at break (%)	Tensile toughness (mJ)
1	56.9	2362.8	2.8	279.1
2	55.1	2426.2	2.8	290.0
3	55.0	2350.5	2.7	270.6
4	55.2	2424.6	2.9	272.0
5	56.6	2429.8	3.0	277.7
Avg.	55.8	2398.8	2.8	277.9
S.D.	0.9	38.8	0.1	7.7

Table D.15 Tensile properties in sheet films of PLA/Talc 5 vol% treated with vinyltriethoyxsilane (VTES)

Sample no.	Tensile strength (MPa)	Young's Modulus (MPa)	Elongation at break (%)	Tensile toughness (mJ)
1	52.7	2280.4	3.3	306.3
2	53.7	2133.1	3.1	364.7
3	50.4	2312.1	3.5	387.3
4	53.8	2186.1	3.4	303.2
5	52.2	2146.1	3.4	357.8
Avg.	52.6	2211.6	3.4	343.9
S.D.	1.4	80.5	0.2	37.4

Table D.16 Tensile properties in thermoforming process of PLA/Talc 5 vol% treated with vinyltriethoyxsilane (VTES)

Sample no.	Tensile strength (MPa)	Young's Modulus (MPa)	Elongation at break (%)	Tensile toughness (mJ)
1	54.4	2179.4	2.9	277.6
2	56.8	2171.7	2.9	269.0
3	56.1	2300.2	2.9	290.6
4	55.7	2167.8	2.9	286.4
5	56.2	2234.6	2.9	266.1
Avg.	55.9	2210.7	2.9	277.9
S.D.	0.9	56.8	0.0	10.6

VITA

Ms. Suphattra Choksriwichit was born in Suphanburi on August 30, 1991. She finished high school at Kanchanapisekwittayalai School, Suphanburi. In 2014, she received the Bachelor's Degree from Department of Chemical Engineering, Faculty of Engineering, Rangsit University. She continued her study for Master's Degree in Chemical Engineering at the Department of Chemical Engineering, Faculty of Engineering, Chulalongkorn University in August, 2014.

In addition, she was invited for poster presentation in Pure and Applied Chemistry International Conference (PACCON 2016). Her title of this presentation was Isothermal cold-crystallization kinetics and morphology of PLA casted film with the incorporation of talc and starch, during February 9-11, 2016 at Bangkok, Thailand.